Uranium isotopes as tracers of groundwater evolution in the Complexe Terminal aquifer of southern Tunisia

Friha Hadj Ammar, Pierre Deschamps, Najiba Chkir, Kamel Zouari, Aissa Agoune, Bruno Hamelin

▶ **To cite this version:**

Friha Hadj Ammar, Pierre Deschamps, Najiba Chkir, Kamel Zouari, Aissa Agoune, et al.. Uranium isotopes as tracers of groundwater evolution in the Complexe Terminal aquifer of southern Tunisia. Quaternary International, 2020, 547, pp.33-49. ⟨10.1016/j.quaint.2020.01.024⟩. ⟨hal-03165195⟩

HAL Id: hal-03165195

https://hal.science/hal-03165195v1

Submitted on 22 Aug 2022

HAL is a multi-disciplinary open access archive for the deposit and dissemination of scientific research documents, whether they are published or not. The documents may come from teaching and research institutions in France or abroad, or from public or private research centers.

L'archive ouverte pluridisciplinaire **HAL**, est destinée au dépôt et à la diffusion de documents scientifiques de niveau recherche, publiés ou non, émanant des établissements d'enseignement et de recherche français ou étrangers, des laboratoires publics ou privés.

Distributed under a Creative Commons CC BY-NC 4.0 - Attribution - Non-commercial use - International License

Version of Record: https://www.sciencedirect.com/science/article/pii/S1040618220300252
Manuscript_74e6e000a394a5334bdf7577b5019dbc

Uranium isotopes as tracers of groundwater evolution in the Complexe Terminal aquifer of southern Tunisia

HADJ AMMAR Friha[a,b✉], DESCHAMPS Pierre[a], CHKIR Najiba[b], ZOUARI Kamel[b], AGOUNE Aissa[c], HAMELIN Bruno[a]

[a] Aix-Marseille Université, CNRS, IRD, Collège de France, CEREGE, Europôle de l'Arbois, BP 80, 13545 Aix en Provence cedex 04, France. frihadj@yahoo.fr, deschamps@cerege.fr, hamelin@cerege.fr. Tel: +216 20 66 44 95; Tel: +33 0442971522.

[b] Sfax University, Laboratory of Radio-Analysis and Environment, National school of Engineering of Sfax, Route de Soukra, BP 1173, 3038 Sfax, Tunisia. frihadj@yahoo.fr, kamel.zouari@enis.rnu.tn.

Tel: +216 20 66 44 95; Tel: +216 74 677 425.

[b] Laboratory of Radio-Analysis and Environment, Faculty of Letters and Humanities, Geography Department, Route El Matar, BP 1168, 3029 Sfax, Tunisia. najiba_chkir@yahoo.fr. Tel: +216 74 670 544.

[c] Ministry of Agriculture and Water Resources, Tunisia. aissa.agoune@iresa.agrinet.tn.

Tel : +216 92 366 489.

[1]

✉Corresponding author: Friha HADJ AMMAR - Laboratory of Radio-Analysis and Environment, National School of Engineering of Sfax, Route de Soukra BP 1173, 3038, Sfax, Tunisia, frihadj@yahoo.fr.

© 2020 published by Elsevier. This manuscript is made available under the CC BY NC user license
https://creativecommons.org/licenses/by-nc/4.0/

Abstract

The Complexe Terminal (CT) multi-layer aquifer is formed by Neogene/Paleogene sand deposits, Upper Senonian (Campanian-Maastrichtian limestones) and Turonian carbonates. The chemical composition and isotopes of carbon and uranium were investigated in groundwater sampled from the main hydrogeological units of the (CT) aquifer in southern Tunisia. We paid special attention to the variability of uranium contents and isotopes ratio ($^{234}U/^{238}U$) to provide a better understanding of the evolution of the groundwater system. Uranium concentrations range from 1.5 to 19.5 ppb, typical of oxic or mildly reducing conditions in groundwaters. The lowest concentrations are found southeast of the study area, where active recharge is supposed to take place.

When looking at the isotope composition, it appears that all the samples, including those from carbonate levels, are in radioactive disequilibrium with significant ^{234}U excess. A clear-cut distinction is observed between Turonian and Senonian carbonate aquifers on the one hand, with $^{234}U/^{238}U$ activity ratios between 1.1 and 1.8, and the sandy aquifer on the other hand, showing higher ratios from 1.8 to 3.2. The distribution of uranium in this complex aquifer system seems to be in agreement with the lithological variability and are ultimately a function of a number of physical and chemical factors including the uranium content of the hosting geological formation, water-rock interaction and mixing between waters having different isotopic signatures. Significant relationships also appear when comparing the uranium distribution with the major ions composition. It is noticeable that uranium is better correlated with sulfate, calcium and magnesium than with other major ions as chloride or bicarbonate.

The ^{14}C activities and $\delta^{13}C$ values of DIC cover a wide range of values, from 1.1 pmc to 30.2 pmc and from -3.6‰ to -10.7‰, respectively. ^{14}C model ages estimated by the Fontes and Garnier model are all younger than 22 Ka and indicate that the recharge of CT groundwater occurred mainly during the end of the last Glacial and throughout the Holocene.

Keywords: CT Southern Tunisia; Uranium isotopes; Radicarbon; Holocene; water-rock interaction; mixing.

1. Introduction

Identification of the parameters controlling the uranium concentration and the origin of the $^{234}U/^{238}U$ fractionation is essential for the potential use of ($^{234}U/^{238}U$) activity ratios as a tracer in hydrogeological investigations. Uranium exists in two oxidation states (U^{IV} or U^{VI}) in groundwater, depending on the environmental conditions. U^{4+} forms insoluble reduced chemical species, while U^{6+} is highly soluble in oxidizing natural waters, occurring as the uranyl cation, and tends to form stable carbonate complexes such as $UO_2 (CO_3)_2^{2-}$ (McKelvey et al., 1955; Langmuir, D., 1978). The concentration and the mobility of uranium isotopes are function of a number of physical and chemical factors including the uranium content of the aquifer rocks and its mineralogical composition, the path lengths and contact time between the aquifer matrix and the flowing water, water-rock interaction and mixing between waters having different isotopic signatures (Riotte et al., 2003; Durand et al., 2005; Maher et al., 2006; Elliot et al., 2014).

Improving our understanding of the interplay of the different factors controlling uranium geochemistry is thus the main topic of this study, carried out on the scale of a large and complex hydrogeological system. The "Complexe Terminal" (CT) aquifer of the Chott basin in southern Tunisia constitutes the main groundwater resource in the study area, characterized by an arid/semi-arid climate with irregular rainfall and very high evapotranspiration rates. In spite of these climatic conditions, oasis agriculture activities based on irrigation have been widely expanded since the second half of the 20th century, strongly increasing the pressure on water resources. Nowadays, the overexploitation of this aquifer system is revealed by spring drying, decreasing piezometric heads, and degradation in water quality (OSS, 2003; Zammouri et al, 2007; Hadj Ammar et al., 2014). Therefore, the ability to use fossil groundwater to buffer arid climate and rainfall deficits is now heavily constrained by the need to protect the groundwater systems. In the current context of climate change and increasing

demand for water, it is essential to understand the groundwater origin, flow dynamics and mean residence times for the assessment of reliability of these resources as a major water supply. A large number of studies have already been devoted to the questions of groundwater residence time and recharge rate over Northern Africa (Guendouz et al., 1997; Edmunds et al., 2004; Baba Sy, 2005; Chkir and Zouari, 2007; Abid et al., 2009; Abid et al., 2010; Hadj Ammar et al., 2010; Abid et al., 2011; Abid et al., 2012; Moulla et al., 2012; Gonçalvès et al. 2013; Hadj Ammar et al., 2014; Petersen et al., 2014; Petersen et al., 2018). However, the precise reconstruction of the groundwater response to climate changes largely remains an open question in this region, still based on limited data sets and models.

Numerous studies have demonstrated the potential use of the $^{234}U/^{238}U$ activity ratio as a tracer of water rock interactions and evolution of groundwater chemistry (Osmond et al., 1974; Andrews et al., 1982; Andrews and Kay, 1983; Pearson et al., 1983; Frohlich and Gellermann, 1987; Ivanovitch et al., 1991; Riotte and Chabaux, 1999; Riotte et al., 2003; Frohlich, 2013; Paces and Wurster, 2014; Méjean et al., 2016), although its use to determine water residence times is generally hampered by the complexities of ^{234}U fractionation. In this respect, several studies have been focused previously on southern Tunisia (Chkir and Zouari, 2007; Chkir et al., 2009; Hadj Ammar et al., 2010; Chkir et al., 2012; Dhaoui et al., 2016), providing us with a still limited dataset, generally related to regional studies on a restricted scale of investigation.

In this paper, we discuss the first comprehensive data set of high precision $^{234}U/^{238}U$ ratios and uranium concentrations measured by thermal ionisation mass spectrometry (TIMS), in groundwater samples from the different aquifer levels of the Tunisian CT. The uranium data are reported and analyzed along with a review of the isotopic composition of water (δ^2H, $\delta^{18}O$), and dissolved carbon (^{14}C and $\delta^{13}C$) measured in the same samples. Our two objectives are first to improve our understanding of the mechanisms controlling the behavior and the

105 isotopic composition of uranium, and thus its potential use as a tracer in groundwater
106 hydrology and chemistry, and second to refine previous descriptions of the CT large-scale
107 circulation flowpaths and paleo-climatic evolution.

108 **2. Description of the study area**

109 The study area is located in southern Tunisia and covers the Chotts basin. This endoreic area
110 is limited to the East by the Tebaga-Kebili and Dahar mountains, to the west by the Algerian
111 border, to the north by the northern upland of the Chotts and Métlaoui upland, and in the
112 South by the Saharan platform (Fig.1).

113 **Fig.1**

114 The geology of the studied area has been investigated elsewhere (e.g. Castany., 1954;
115 Burollet., 1956; Busson., 1970; Zargouni et al., 1985; Bouaziz., 1995) and we will only recall
116 here the information relevant to the present work. Embedded under the Chott basin, the North
117 Western Aquifer System (NWAS) consists of two principal deep aquifers, the Continental
118 Intercalaire (CI) and the Complexe Terminal (CT), and of Quaternary shallow phreatic
119 aquifers. The CI is a multi layered aquifer composed of a succession of different sedimentary
120 series of late Jurassic to early Cretaceous detrital sediments, separated by gypsum
121 intercalation and clayey levels (Busson, 1967; Bouaziz, 1986). The groundwater reservoir of
122 the CI is contained in sandstone strata of Albo-Aptian and barremian deposits.
123 The formations which host the intermediate Complexe Terminal aquifer are Upper Cretaceous
124 carbonates and Paleogene/Neogene sands. These Upper Cretaceous strata, which are
125 dominated by mudstones, evaporites and carbonates, are overlain by Paleocene and Eocene
126 successions consisting of clays, calcareous shales with interbedded layers of gypsum,
127 dolomite and phosphatic limestones (Zouaghi et al., 2005). In some areas, Paleocene and
128 Eocene deposits constitute the substratum of the Mio-Pliocene sandy strata which, together
129 with the Upper Cretaceous carbonates, form the principal formations of the intermediate

130 Complexe Terminal aquifer (Burollet, 1956; Biely et al., 1972; Mannai-Tayech, 2009).
131 Elsewhere in the east of the Tozeur region, Mio-Pliocene sequences overlie unconformably
132 the Upper Cretaceous strata due to the erosion of the Paleocene and Eocene deposits
133 (Chaabani, 1995; Kamel, 2007). The Miocene series are overlain by Pliocene to Quaternary
134 continental deposits known as the Segui Fm that consists of a gypseous silty to sandy
135 succession becoming conglomeratic at the top and constitutes the upper shallow aquifer
136 (Castany, 1954; Burollet, 1956; Zargouni et al., 1985; Tlig et al., 1991).

137 Conceptual block diagrams showing the different hydrostratigraphic units have been
138 elaborated to define the layering of the different aquifers and their connectivity, by
139 considering lateral facies changes and local tectonic structures (Fig.2.a and b).

140 The CT aquifer system is characterized by large changes in facies and thickness from North to
141 South and from East to West. The CT multi-layer aquifer is present both under the Nefzaoua
142 basin where it is hosted in Upper Senonian and Turonian carbonate formations (Fig.2.a) and
143 under the Djerid basin where Mio-Pliocene sands of Redjime Mâatoug, Tozeur and Chott
144 Gharsa plain constitutes the main aquifer level (Fig.2.b).

145 The Senonian and Turonian formations become deeper in the Djerid basin. The Senonian ones
146 are directly overlain by the Mio-Pliocene sands in the East of Tozeur region, while further
147 West, they are separated by phosphatic Eocene limestone strata (ERESS, 1972; Zargouni et
148 al., 1985). The Turonian consists of fractured and karstified dolomite/limestone with a mean
149 thickness of about 50 m. Groundwater flows mostly from Southeast to Northwest, broadly
150 from the Dahar mountains which constitute the main recharge area, to the main discharge area
151 in the Chott Djerid depression (Fig.1) (ERESS, 1972; OSS, 2003; Zammouri et al., 2007,
152 Hadj Ammar et al., 2014).

153 In the Djerid basin, Mio-Pliocene formations outcrop at the Tozeur uplift and become deeper
154 to the West of the basin. In this basin, groundwater flows from the southwestern Algerian
155 Great Oriental Erg, from the northern upland of the Chotts and from the Metlaoui upland.
156 Discharge areas are located in both the Chott Djerid and Chott Gharsa depressions (Fig.1)
157 (Edmunds et al., 1997; Kamel et al., 2007; Hadj Ammar et al., 2014).

158 The CT aquifer is confined over the majority of the Nefzaoua and Djerid basin. In fact, the
159 geological formations of the CT aquifer are overlain by clayey impermeable and/or sandy-
160 clayey semi-impermeable layers that restrict the vertical movement of water and thus, mixing
161 with water from the shallow aquifer is limited. However, at the proximity of faults,
162 preferential vertical leakage can occur between sandstones and carbonate layers of the CT
163 system as well as between the deep CI or the shallow aquifers and the CT system (Fig.2.a and
164 b). Only in the recharge area of Douz-Jemna regions of Nefzaoua basin and Kriz-El Hamma-
165 Degache areas of Djerid basin, the CT aquifer is under non-confined conditions. A possible
166 exchange between the CT and the shallow aquifer can thus occur in these locations (ERESS,
167 1972; Mamou, 1990; Kamel et al., 2007; Zammouri et al., 2007).

168 **Fig.2**

169 Historically, most of CT wells were artesian. Over the last two decades, an increasing
170 withdrawal for agriculture, industry and domestic uses have led to the overexploitation of
171 groundwater resources and caused a general drop of the water table (OSS, 2003). Nowadays,
172 only a few wells are still artesian.

173 ## 3. Sampling and analytical method

174 The main hydrogeological units of the study area have been sampled during the spring season.
175 Three boreholes (#1, #2 and #3) from the Turonian aquifer level, twenty one samples from the
176 Senonian limestone aquifer (#4, #5,…, #24), seven boreholes from the Mio-Pliocene aquifer

177 of Redjime Mâatoug (#25, to #31), twenty four boreholes from the sandy Mio-Pliocene
178 aquifer of Tozeur (#32, to #55) and eleven boreholes from sandy Mio-Pliocene aquifer of
179 Chott El Gharsa plain (#56, #57, …, #66) were sampled. The sampling grid has been chosen
180 as representative of the entire basin (Fig.1). We paid special attention to sample the different
181 lithological formations, at different depths, and cover the recharge and discharge zones of the
182 multi-layer aquifer.
183 All samples were collected directly from the well-head of currently exploited boreholes.
184 Groundwater was pumped until stabilization of temperature, pH and EC before sampling.
185 Screened interval depths mentioned in Table 1 correspond to the top of the screen.

186 Groundwater samples were filtered through 0.45µm acetate cellulose filter. Temperature,
187 electrical conductivity and pH were measured on site using a HI 9828 Multi-parameter probe.
188 Samples for the determination of the major element concentrations, as well as uranium
189 isotopic composition were stored in polyethylene bottles previously cleaned with diluted nitric
190 acid and distilled water and rinsed three times with sampled groundwater prior to filling.
191 Nitric acid was added to aliquots devoted to cations analyses. Volumetric titrations were
192 performed for the determination of bicarbonate alkalinity. Samples for radiocarbon analyses
193 were collected in the field by precipitating dissolved inorganic carbon as $BaCO_3$ from 100-
194 150 L sample volume, depending upon the alkalinity of each sample. The precipitates were
195 preserved in polyethylene bottles.
196 Major element concentrations, as well as water stable isotopes and ^{14}C activities, were
197 measured at the Laboratory of Radio-Analysis and Environment of the National School of
198 Engineering of Sfax (Tunisia). Cations were analyzed with a ion chromatography equipped
199 with columns IC-PakTM CM/D for cations, using EDTA and nitric acid as eluent, and anions
200 with a Metrohm chromatograph equipped with columns CI SUPER-SEP using phthalic acid

and acetonitric as eluent. The overall detection limit for each major element was about 0.04 mg/l. For each analysis, the ionic balance was lower than 5% (Table 1).

Table 1

Analyses of stable isotope ratios (^{2}H and ^{18}O) were performed by Laser Spectrometry with a LGR DLT100 instrument (Penna et al., 2010) and reported in ‰ vs VSMOW standard (Vienna-Standard Mean Oceanic Water) with a precision of ±0.1‰ for ^{18}O and ±1‰ for ^{2}H (Table 2).

Radiocarbon activities were determined by benzene synthesis and liquid scintillation spectrometry. Radiocarbon activities are reported as percent of modern carbon (pMC) (Stuiver and Polach, 1977) with uncertainties of ±1 pMC. Aggarwal et al. (2013) demonstrated that uptake of atmospheric CO_2 may occur during the on-site precipitation procedure on large volume alkaline samples, resulting in contamination by modern ^{14}C potentially as high as 1 to 10 pMC. This represents an important caveat on our data that must therefore be discussed with caution.

The $^{13}C/^{12}C$ ratios were determined by isotope ratio mass spectrometry at the IAEA and CEREGE laboratories. Results are reported as δ values relative to VPDB (Vienna Pee Dee Belemnite) standard. The ^{13}C uncertainty is of ±0.3‰ (Table 2).

Uranium isotopic compositions were determined by Thermal Ionization Mass Spectrometry (TIMS; VG54-30) at CEREGE. For each sample, 200 ml were weighed and spiked with a $^{233}U/^{236}U$ spike. After preconcentration by coprecipitation of iron oxy-hydroxyde, uranium was separated and purified using UTEVA resin (Uranium and TEtraValents Actinides) conditioned with nitric acid. The solution was evaporated, and the sample loaded on a single rhenium filament with colloidal graphite. Masses 233, 234, 235 and 236 were measured in peak-jumping mode on a VG54-30 mass spectrometer equipped with an ion-counting Daly detector and a 30 cm electrostatic analyser. The activity ratio ($^{234}U/^{238}U$) was calculated by

assuming the natural value of 137.88 for the $^{238}U/^{235}U$ atomic ratio (Condon et al. 2010). The uncertainties of the $^{234}U/^{238}U$ ratios were generally about 5‰ except for a few samples, for which it could reach 9‰. The reproducibility of the U isotopic analyses was assessed with replicate analyses of one sample ("Jemna" sample), which all agreed within error, and yielded a mean value of $(^{234}U/^{238}U) = 1.668 \pm 0.004$ (2σ, n = 3). Total blanks for uranium were better than 20 pg, thus negligible compared to the U amounts analysed in the sample (Table 2).

Table 2

4. Results

Hydrochemical, stable isotopes content and ^{14}C data, together with the uranium concentrations and the $(^{234}U/^{238}U)$ activity ratios are reported in Table 1 and Table 2.

4.1.Geochemical characteristics of CT groundwater

The major processes controlling the CT groundwater chemistry have been investigated in previous studies (e.g., Abid et al., 2011, Jarraya et al., 2013, Hadj Ammar et al., 2014; Hadj Ammar, 2016). In this paper, only specific features that could affect uranium geochemistry will be highlighted. TDS values are ranging from 648 to 6290 mg/l and the major ions are in the following order of contribution: calcium, sodium, chloride, sulfate, magnesium, potassium and bicarbonate. Groundwater is mostly of the Na^+-$Cl^-(SO_4^{2-})$ and $Ca^{2+}(Mg^{2+})$-$Cl^-(SO_4^{2-})$ types. Groundwater geochemistry is controlled by water/rock interactions, mineral dissolution and ion exchange (Hadj Ammar et al., 2014). The majority of water samples are dominated by the dissolution of gypsum and halite, revealed by correlations between $[Ca^{2+}]$ and $[SO_4^{2-}]$ or between $[Na^+]$ and $[Cl^-]$ among various sets of samples, and are saturated with respect to dolomite and calcite precipitation (Table 1). High concentrations of the major ions observed in some localities are explained by vertical mixing between surface and/or deep natural saline water, induced by anthropogenic activities (Hadj Ammar et al., 2014).

4.2.Dissolved uranium and $^{234}U/^{238}U$ ratio in CT groundwaters

The results are illustrated in Figure 3, as $^{234}U/^{238}U$ activity ratios plotted versus 1/[U] $(ppb)^{-1}$. Some of the main U-results are indicated along two representative cross-sections along a generalized flow path in both Nefzaoua and Djerid basin (Fig.4a, b).

Uranium concentrations show a large variability from 1.5 to 19 ppb.

Fig.3

Most samples are in fact below 8 ppb, except four samples from the Mio-Pliocene sand aquifer (#53 and #54 in Tozeur basin, and #57 and #62 in the Chott El Gharsa plain). The lowest concentrations are found in two samples from the Senonian (#14 and #18) closest to the aquifer outcrop in the Dahar mountain (Fig.4a), where active or recent recharge has been identified by previous studies (Edmunds et al., 2003, Guendouz et al., 2003; Abid et al., 2010; Abid et al., 2011). By contrast, the Turonian aquifer sample which is also located in this recharge area, furthest to the East in the Dahar mountain, is among the highest uranium content (#1, 8 ppb). These concentrations are in the upper half of the global distribution of dissolved uranium in continental waters (Ivanovitch and Harmon, 1992), although without extremely high values as high as 10-100 ppm sometimes encountered in uraniferous environments. Such intermediate range is generally considered as associated with oxic or mildly reducing conditions (Méjean et al., 2016; Riedel and Kübeck, 2018). By comparison we measured much lower concentrations in the CI aquifer, well below 1 ppb and down to our blank level, in the anoxic deepest regions of the basin (Chkir and zouari, 2007; Chkir et al., 2009, 2012; Pertersen et al., 2013).

The $^{234}U/^{238}U$ activity ratios are all greater than one, ranging from 1.1 to 3.2. Thus, it appears that all the samples, including those from limestone levels, are in radioactive disequilibrium with excess of ^{234}U. A clear-cut distinction is observed between the Turonian and Senonian

carbonates aquifer, on the one hand, with $^{234}U/^{238}U$ activity ratios between 1.1 and 1.8, and the Mio-Pliocene aquifer from Tozeur on the other hand, with higher ratios from 1.8 to 3.2. Also noticeable is the striking contrast between the two groups of samples from the Mio-Pliocene aquifer, as the samples from Chott El Gharsa plain, by contrast with those from Tozeur basin, all cluster at the low $^{234}U/^{238}U$ and high [U] end-member in the diagram of Figure 3, with the only exception of sample #58 at $^{234}U/^{238}U = 2.8$.

The highest $^{234}U/^{238}U$ activity ratios correspond to samples #36 and #52 of the Mio-Pliocene sand close to Tozeur uplift, and also to sample #25 of Mio-Pliocene in the western part of the Redjime Mâatoug region (Fig.4b).

Fig.4

4.3.Stable isotopes and groundwater ages

The stable isotope data of the same samples as in this study have been reported previously by Hadj Ammar et al., 2014. $\delta^{18}O$ ranged from -7.8‰ to -4.2 and $\delta^{2}H$ from -57.4‰ to -34.8‰, with mean values of (-6.0 ± 0.2‰) and (-46.1 ± 1‰) respectively (Table 2). This isotopic variation in CT groundwaters is controlled dominantly by evaporation processes, paleo-recharge and mixing between waters with different isotopic ratios (Fig.12 in Hadj Ammar et al., 2014).

Radiocarbon activities and $\delta^{13}C$ values of DIC determined for 34 water samples cover a wide range from 30.2 to 1.1 pmc and from -10.75 to -3.6‰, respectively (Table 2, Fig.5) (this work, and Abid et al., 2011; Abid et al., 2012; Yangui et al., 2012). The relatively high $\delta^{13}C$ values shows that dissolution of solid carbonate and carbon exchange between DIC and carbonate minerals are the dominant processes affecting the $\delta^{13}C$ and ^{14}C content of DIC in the CT groundwater.

Fig.5

A large number of correction models, relying on various assumptions, have been proposed in the literature for dating groundwater with radiocarbon, in order to account for the different processes which may affect the ^{14}C activity through dissolution/precipitation processes with the basement lithology, or exchange with the gas phase in the unsaturated zone (Ingerson and Pearson, 1964; Evans et al., 1979; Fontes and Garnier, 1979; Salem et al., 1980; Eichinger, 1983; Clark and Fritz, 1997, Buckau et al., 2000a; Zhu and Murphy, 2000; Geyh, 2000, 2005; Han and Plummer, 2013, 2016).

The models cited above have been widely applied and discussed in the literature and are therefore not discussed in detail here. In this study, we used the model of Fontes and Garnier (1979) which takes into account the dissolution and precipitation of carbonates and evaporites, the Ca/Na ion exchange process on clay minerals and the transition from open to closed conditions for carbonate dissolution. A detailed explanation on the choice of this model among the others and the following C signatures used to calculate radiocarbon ages of southern Tunisia groundwaters were well discussed in Abid et al., 2012, 2014. The model ages that we obtain are listed in Table 2 and illustrated as a frequency histogram based on Gaussian distribution analysis within a (±3σ) interval (Fig.6). Although widely scattered between 1.5 and 25 ka, the distribution of model ages seems to show two main broad clusters centered around 5 ka and 13 ka respectively. The youngest ages (1.5 – 2.5 ka) are found in Senonian and one Turonian samples, and the oldest (19 – 25 ka) are all from the Tozeur basin Miocene aquifer.

Fig.6

5. Discussion

Each of the five regional aquifers studied here show a distinct pattern in the $^{234}U/^{238}U$ versus 1/[U] diagram of Figure 3.

5.1. Southern aquifers: Nefzaoua and Redjime Mâatoug

For the two aquifers from the southern part of the basin, i.e. Senonian from Nefzaoua basin and Miocene from Redjime Mâatoug, a clear geographical repartition is noted in the data (Fig.4, Fig.7). In the first case, U-concentration increases along the groundwater pathway inferred from the piezometry, as the aquifer deepens away from the recharge area in the Dahar Mountain (#14 and #18), down to sample #15 and #17 to the north, #16 to the north-east, #12 to the south-west. Similarly, the lowest concentrations are found in the eastern part of Redjime Mâatoug (#31 and #29), under the southern edge of Chott El Djerid, whereas higher values are found further west, although in this second case with no clear relationship to present-day piezometry.

Fig.7

Similar increases have been interpreted classically in various previous studies around the world (e.g. Arendt et al., 1980; Spalding and Druliner, 1981) as resulting from progressive dissolution of the basement rock along the transit of the groundwater. This explanation is consistent with our data and is coherent with the observation that uranium is well correlated with the total dissolved ions, and particularly with sulfate ($0,31<R^2<0,91$) and calcium ($0,69<R^2<0,75$) (Fig. 8). Dissolution of gypsum and anhydrite have been suggested as a dominant control of these groundwaters chemistries, especially in the case of Redjime Mâatoug where [Ca^{2+}] and [SO_4^{2-}] are strongly correlated (Hadj Ammar et al., 2014).

Fig.8

The hypothesis that uranium could be associated with sulfate bearing evaporites must thus be considered and would deserve further testing on the solid phase. Nevertheless, it must also be noted that Nefzaoua groundwaters show systematically higher [U]/[Ca^{2+}] and [U]/[SO_4^{2-}] ratios than Redjime Maatoug in Fig.8, suggesting that more than one mineral phase is

347 releasing uranium to the solution. Indeed, for the Senonian groundwaters, the calcareous
348 lithology of the basement is expected to make a significant contribution to the dissolved
349 uranium content (e.g. Bonotto and Andrews, 2000). Other mechanisms are often advocated as
350 possible control factors of the water chemistry, such as dedolomitization or cation exchange
351 on bedrock surface (Hiscock, 2005; Chae et al., 2006; Escorcia et al., 2013; Luo et al., 2018).
352 However, neither of these two processes is apparent in our data, as suggested by the absence
353 of correlation between [U] and the Mg/Ca ratio, nor with the Na/Ca ratio (not shown).

354 Moreover, in both aquifers, the geographical trend is far from regular, with the highest
355 concentrations observed in intermediate positions along the transects, which suggests
356 heterogeneous and patchy distribution of the basement lithology, and also likely irregular
357 pathways and variable flow rates of the groundwater circulation.

358 By contrast with their comparable features for uranium concentrations, the two southern
359 aquifers show very contrasted trends in isotopic composition. The $^{234}U/^{238}U$ ratio increases
360 regularly in the Redjime Mâatoug samples along the concentration gradient, up to one of the
361 highest values in our data set (# 25: $^{234}U/^{238}U = 3.1$) (Fig.4b), while the Senonian samples do
362 not show such evolution with values randomly scattered within a narrow band between 1.5
363 and 1.8, except for sample #18 close to equilibrium ($^{234}U/^{238}U = 1.1$) (Fig.4a). The ^{234}U
364 excess is typical of all surface and underground continental waters and is a fairly well-known
365 phenomenon since the early compilations of Ivanovitch and Harmon (1992). It has been
366 documented in numerous environments, although comparatively less often in limestone
367 aquifers (Osmond and Cowart, 1976; Andrews and Kay, 1983; Osmond and Ivanovich, 1992;
368 Gascoyne, 1992; Davis and Krogh, 2001; Paces et al., 2002; Porcelli and Swarzenki, 2003;
369 Chabaux et al., 2003, 2008; Smedley et al., 2006). Our data from the Senonian limestone
370 aquifer are thus interesting in two main aspects: first they confirm the isotopic disequilibrium
371 of uranium dissolved from calcareous formations, showing that α-recoil processes are also

significant in such facies even though water-rock interaction mainly occurs as congruent dissolution. Second, we do not observe the decreasing trend of $^{234}U/^{238}U$ with increasing uranium content which was described in several studies (Kronfeld and Adams, 1974; Osmond and Coward, 1976; Burkitbayev et al., 2012). This inverse trend is generally interpreted as reflecting progressive dampening of the ^{234}U fractionation due to alpha recoil by the increase in uranium at secular equilibrium released as weathering increases. Instead, this constant $^{234}U/^{238}U$ ratio suggests that the ratio between the rate of removal of ^{234}U from the rim of rock affected by alpha recoil, and the rate of bulk chemical dissolution remains constant along the groundwater pathway, as expected in a homogeneous basement (Fig.4a).

By contrast, the interpretation is more complex for the Mio-Pliocene aquifer from Redjime Mâatoug, where the ^{234}U preferential leaching increases with [U] (Fig.4b) . A possible simple explanation could advocate mixing in various proportions between two groundwater end-members with contrasting composition, related to the type of dominant basement rock encountered along their pathway, e.g. carbonates for the (low [U]-low $^{234}U/^{238}U$) end-member, and evaporite (mostly of sulfate-bearing type) for the (high [U]-high $^{234}U/^{238}U$) end-member. Under this assumption, the regional trend observed in the data would reflect a progressive increase of the proportion of evaporites within the aquifer reservoir along the East-West gradient of the Redjime Maâtoug basin.

5.2. Northern sectors: Chott El Gharsa plain and Tozeur ridge

Compared to the two southern aquifers, the two northern Mio-Pliocene sandy aquifers show more complex patterns, and quite different from each other.

On the one hand, the seven samples from the Mio-Pliocene of the Chott El Gharsa plain all plot in a relatively restricted domain in Figure 3, corresponding to the (high [U], low $^{234}U/^{238}U$) end-member, similar to the most enriched Senonian and Turonian samples: two of these samples (#57 and #62), along with one of Turonian age, bear indeed the lowest

397 $^{234}U/^{238}U$ in our study. The similarity between the sandy aquifer of Chott El Gharsa plain and
398 the calcareous layers further South is unexpected. This seems to suggest counter-intuitively
399 similar U-bearing phases and similar duration of water-rock interaction in both cases. The
400 flow lines inferred from the present piezometry indicate a circulation oriented to the South in
401 this region, and thus a recharge further North, possibly around the Metlaoui upland. The
402 transit distance of the groundwater is thus probably comparable with that of the southern
403 aquifers, and the depth of collection significantly deeper (500-1100 m depth), thus possibly
404 coherent with longer residence times and higher dissolved mineral load.

405 Finally, the 24 samples collected from the sandy aquifer along the Tozeur uplift and the
406 Tozeur basin show the widest dispersion in Figure 3, encompassing both the highest results in
407 $^{234}U/^{238}U$ ratios (#36 and 52) and highest [U] (#53 and 54), but also samples trending towards
408 the depleted end-member (#33, 35, 38 and 48), or towards the (high [U], low $^{234}U/^{238}U$) end-
409 member (#40 and 45), although all samples but one have $^{234}U/^{238}U$ ratios higher than 2. Such
410 a large diversity must be related to the complex geomorphology and tectonic structure of the
411 Tozeur uplift that is bordered or crossed by several large faults and which represents the
412 surface expression of a large uplift of the sedimentary strata at depth (Fig. 2.b). Moreover, the
413 Tozeur region is also known for a complex hydrogeological context, resulting in upwelling of
414 deep-seated groundwater attested by the occurrence of numerous springs and artesian wells
415 before the recent exponential increase of the extraction for human activities. Although widely
416 scattered in terms of spatial repartition, the results show nevertheless some significant
417 groupings. For instance, the four most depleted samples (#48, 38, 33 and 35) are all clustered
418 on the southern slope of the Tozeur uplift, in the north-eastern region (Fig.1, Fig.3 and
419 Fig.4a). These samples follow the same trend as that defined by those from Redjime Mâatoug
420 and seem to correspond to initial stages of evolution. This may mean either close proximity to
421 recharge sites, or slower recharge rates, or alternatively a basement lithology depleted in the

(high $^{234}U/^{238}U$, high [U]) source rock, supposedly associated with sulfates in the case of Redjime Mâatoug.

Similarly, another series of samples located further West in the Tozeur plain (# 36, 52, 46, 37) are regularly spaced along a linear trend between the (high $^{234}U/^{238}U$, high [U]) and (low $^{234}U/^{238}U$, high [U]) end-members. This suggests that the two types of waters sustaining these end-members, i.e. represented at the end of the Redjime Maâtoug transect on the one hand, and under the Chott El Gharsa plain on the other, are also present under the Tozeur plain and mix in various proportions either along strata or through inter-layers connections.

Finally, a last noticeable observation is that the two samples most enriched in uranium (#53 and 54), which lie clearly above the general correlation between [U] and TDS in Fig. 8, are associated with the phosphate ore of Tozeur-Nefta located on the northern edge of the Tozeur ridge (Fig. 1) and embedded in Eocene layers directly underlying the Miocene CT aquifer (Gallala et al., 2016). These phosphates are rich in uranium (35 ppm, Sassi, 1974; Chaabani, 1995). Uranium is known to have a high affinity for phosphates, as well as for carbonates, which can also exert a strong control on its behavior in solution (Sandino and Bruno, 1992; Adam et al., 2011; Beazley et al., 2011; Schipper et al., 2011; Alloway, 2013; Mehta et al., 2014; Cumberland et al., 2016). As for the previous examples, the contact between the groundwater and the source rock must be very localized, along fractures or channels, since sample #50, also very close to the same site, do not show the same enrichment. Again, experimental leaching experiments on solid phases, as well as phosphorus measurements in the waters would be necessary before a definite interpretation of these results.

5.3.Uranium concentrations and isotopes versus major element chemistry

In addition, it is worth underlining that the different trends discussed above, based on uranium content and isotopic ratio, do not correspond to equivalent grouping in major element composition. The chemical results are indeed randomly scattered between the 1) dilute

447 recharge waters, 2) sulfate end-member and 3) chloride end-member, reflecting the main
448 control of evaporites dissolution on the groundwater chemistry (Hadj Ammar et al., 2014).
449 The four regional aquifers discussed above show large overlaps in their chemical signatures,
450 and the sulfate and chloride types are both represented in each of them. The Chott El Gharsa
451 samples are all in the upper range of total dissolved ions, the Tozeur uplift samples are highly
452 dispersed, and the most dilute samples are found in the Senonian Nefzaoua samples and
453 Miocene Redjime Mâatoug in the south-eastern region. There is no general correlation
454 between the uranium concentration and any of the major ions, except for the qualitative
455 observation already noted above that the highest [U] also correspond to the highest sulfate
456 contents (# 53, 54, Fig. 8). By comparison, samples most enriched in Cl, like Mio-Pliocene
457 #39 and #43, or in Ca like # 36 and #39, are not particularly rich in dissolved uranium (Fig.8).

458 Finally, a remarkable feature of these data is that the high $^{234}U/^{238}U$ end-member samples,
459 such as Mio-Pliocene #36 and #52 of the Tozeur basin, or Mio-Pliocene #25 of the Redjime
460 Mâatoug region, do not bear any particular chemical signature in their major ion composition
461 (Fig. 4b, Fig. 8). High $^{234}U/^{238}U$ ratios have often been interpreted as resulting from a
462 downstream position of the sample with respect to a redox-front across the aquifer (Osmond
463 and Cowart, 2000; Petersen et al., 2013; Méjean et al., 2016), where the alpha-recoiled ^{234}U
464 continues to be leached out of the basement rock while uranium has been quantitatively
465 depleted by precipitation in the reductive environment. However, this interpretation seems to
466 be ruled out in the case of the CT groundwaters, characterized generally by medium or high
467 uranium contents typical of oxic conditions. A possible clue lies in the observation that all the
468 samples with large ^{234}U excess are located in upstream positions with respect to present-day
469 piezometric lines (see Fig.1), as already noted for the Tozeur basin data, suggesting that the
470 radioactive disequilibrium might be linked to the early phase of water-rock interaction within
471 sandstone aquifers, although this hypothesis requires obviously further verification.

5.4. Chronological and paleoenvironmental inferences

Paleoclimatic studies revealed the occurrence of several humid phases over the entire Mediterranean basin during the last glacial-interglacial cycle, based on marine sediments (Fontugne et al., 1994), foraminifera (Kallel et al., 2000; Essallami et al., 2007), lacustrine records (Ariztegui et al., 2000; Causse et al., 2003), and stalagmites (Genty et al., 2003, 2006; Braun et al., 2019). Groundwaters may also constitute to some extent archives of these climate oscillations. For instance, Petersen et al. (2014) showed that the distribution of cosmogenic ^{36}Cl along the South Saharan CI pathway is strongly controlled by the alternation of dry and humid phases, and that the last interglacial period must have been particularly humid. This finding is strongly supported by 14C measurements which are below the detection limit that indicate residence times greater than 35 ka.

Our $\delta^{18}O$ and $\delta^{2}H$ data in the southern Tunisian CT (Hadj Ammar et al., 2014) showed that the aquifer was recharged with water more depleted in heavy isotopes than present-day precipitation, as generally observed in deep groundwaters over the whole Northern Africa. This observation is also coherent with the recharge temperatures lower by 2-3°C than present, estimated from noble gas paleothermometry in CT groundwater from Algeria (Guendouz et al., 1997; Stute and Schlosser, 1993).

Our data also demonstrated that the different regional aquifers of the CT suffered from various degrees of evaporation, indicating different hydroclimatic conditions upon recharge. Specifically, the Chott El Gharsa CT groundwaters showed more depleted isotope signatures than the other regions, close to the global meteoric water line, a characteristic shared with three Senonian and with the Turonian samples (Fig.9). This similarity was already noted with the uranium results, these samples constituting together the (low $^{234}U/^{238}U$, high [U]) end-member in Figure 3. This confirms the striking contrast between the groudwaters from the different sandy Mio-Pliocene aquifers, and the possible synchroneity between the Nefzaoua

497 and Chott El Gharsa recharge. By contrast, all the other regions are scattered towards less
498 depleted values along a common evaporation trend.

499 **Fig.9**

500 Both the stable isotope compositions and the ^{14}C activities of our samples are thus consistent
501 with recharge periods scattered over the Holocene and Late Pleistocene. ^{14}C model ages,
502 although strongly model-dependent and prone to contamination bias, show a noticeable
503 geographical repartition with younger model ages located in the south-eastern Senonian
504 aquifer, thus compatible with the general circulation pattern inferred from present-day
505 piezometry, which suggests a SE-NW flow path originating from the Dahar. At the other end,
506 the oldest ^{14}C model ages are scattered in the deepest regions of the basin, on the northern
507 edge of Chott El Gharsa and under the Tozeur plain and Tozeur uplift (Fig.6 and Fig.10).

508 On the other hand, the ^{14}C activities measured in the samples from the Dahar upland is only
509 slightly lower than 30 pMC, which indicates either an early Holocene recharge, or mixing
510 between a small fraction of modern recharge with more ancient waters. The second
511 hypothesis seems to be confirmed by the presence of low but detectable environmental tritium
512 contents in samples #14 (0.7 TU) and #18 (0.45 TU) (Hadj Ammar, 2016). The low ^{14}C
513 activity was also observed in one sample collected from the nearby outcrop of the CI by
514 (Petersen et al. 2018). The high $\delta^{13}C$ values measured in all our samples, including those with
515 the youngest ^{14}C model ages, also demonstrates that the addition of dead carbon leached out
516 of the carbonates from the reservoir formation happens early during the groundwater
517 percolation along the aquifer layer.

518 **Fig.10**

519 As detailed above in the different regional discussions, we do not identified any general
520 correlation between the uranium trends and these broad scale characteristics of the aquifer. In

521 particular, our data do not seem to corroborate the conclusions from recent studies correlating
522 uranium concentrations and $^{234}U/^{238}U$ activity ratios with the ^{14}C activities and residence time
523 (Kronfled et al., 1994; Malov, 2013; Malov et al., 2016), who found that groundwater with
524 lower residence time, have enriched $\delta^{18}O$ and $\delta^{2}H$ values and lower $^{234}U/^{238}U$ ratios.
525 Therefore, the complexities described above in the uranium isotope variations preclude their
526 use as a chronometer in this case as in most previous studies around the world, although with
527 several exceptions in very specific situations (e.g. Chalov et al., 1964, 1970; Kronfeld and
528 Adams, 1974; Andrews and Kay, 1978; Andrews et al., 1982).

529 **6. Conclusion**

530 We have produced in this study the largest data set available so far of uranium concentrations
531 and $^{234}U/^{238}U$ isotopic ratios in the Complexe Terminal of the Sub Saharan Aquifer System,
532 with samples representative of the full variety of lithological reservoirs and hydrological
533 situations encountered in this large-scale groundwater aquifer. The results show a large range
534 of variation, both for Uranium concentration (factor 13 between the most dilute and most
535 enriched samples), and for $^{234}U/^{238}U$ values, with all samples out of secular equilibrium with
536 excess ^{234}U ranging from 1.1 to 3.2. Moreover, the different regional sub-systems are
537 characterized by different trends clearly distinct from each other, by contrast with the major
538 ions chemistry which shows large overlaps. As a whole, the results are scattered among three
539 end-members: 1) (low [U], low $^{234}U/^{238}U$) typical of the southeastern samples closest to the
540 Dahar recharge area; 2) (high [U], low $^{234}U/^{238}U$) found in the Senonian and Turonian mostly
541 carbonated aquifer layers, and in the Miocene sandstone from the Chott El Gharsa; and 3)
542 (high or intermediate [U], high $^{234}U/^{238}U$) identified in some samples from the Redjime
543 Mâatoug Miocene sandstone in the Southwest region, and in the Miocene from the Tozeur
544 area. The origin of those variations remains largely speculative, awaiting for a definite
545 identication of the specific uranium bearing solids in the basement rock related to the different

546 end-members. In this respect, future investigations should probably aim at revisiting
547 experimental leaching of solid phases from drill cores, when available, with a special attention
548 to sulfate and phosphate bearing phases. Of particular interest is the observation that all the
549 groundwater samples from the limestone-dominant layers of the Senonian and Turonian are in
550 radioactive disequilibrium, seemingly unexpected as carbonate weathering is generally
551 considered mostly as a congruent dissolution process. The $^{234}U/^{238}U$ ratios are not correlated
552 with the concentration in uranium in this part of the CT, in contrast with previous studies in
553 other regions of the world, suggesting in this case a constant ratio between the uranium
554 addition due to weathering, and ^{234}U enrichment from alpha recoil. The exact mechanism of
555 this enrichment remains thus to be elucidated, linked either to the carbonate itself, or minor
556 phases, or even surface exchange reactions. On the other hand, the high $^{234}U/^{238}U$ values,
557 higher than 1.8 are only found in the groundwaters from the Miocene sandstones, in a patchy
558 distribution probably related to the highly heterogeneous lithology of the basement rocks.

559 More generally, no simple correlation is found between the hydrological features of the CT
560 and the uranium signature of the groundwaters, except in the upstream regions of the path-
561 flow closest to the Dahar recharge area. While ^{14}C model ages are broadly consistent with a
562 SE-NW direction of the grounwater circulation, coherent with the dipping of the sedimentary
563 layers in the basin, alternatively high or low $^{234}U/^{238}U$ values can be found in the deepest parts
564 of the aquifer.

565 Based on radiocarbon model ages and isotopic signatures, we infer that recharge of the CT
566 aquifer occurred during different climatic conditions compared to the present day. This
567 paleorecharge extended from the end of the last glacial to the Holocene periods.

568 In spite of the number of questions remaining unanswered at this stage about its behaviour,
569 the results of this study confirms that uranium bears a wealth of original informations about

570 the groundwater chemical evolution, and thus should desserve a dedicated attention in future
571 research in chemical hydrology.

572 **Acknowledgements**

573 The authors are most grateful to CRDA for access to the sampling sites on the field, and to
574 both technical staff of *Centre de Recherche et d'Enseignement de Géosciences de*
575 *l'Environnement* CEREGE and of the Laboratory of Radio-Analysis and Environment for
576 their excellent operation during uranium isotopic compositions, and chemical and isotopic
577 analysis. The authors thank the LABEX OT-Med (Objectif Terre: Bassin Méditerranéen;
578 http://www.otmed.fr/) for financial support to the first author. This works also benefit from
579 the EQUIPEX project ASTER-CEREGE. Very constructive criticisms and benevolent review
580 from Daniele Pinti and two anonymous reviewers have been much helpful and were deeply
581 appreciated.

582 **References**

583 **A**bid, K., Trabelsi, R., Zouari, K., Abidi, B., 2009. Caractérisation hydrogéochimique de la
584 nappe du Continental Intercalaire (sud tunisien)/Hydrogeochemical characterization of the
585 Continental Intercalaire aquifer (southern Tunisia). *Hydrological Sciences Journal, 54, 526-*
586 *537.*

587 **A**bid, K., Zouari, K., Abidi, B., 2010. Identification and characterisation of hydrogeological
588 relays of continental intercalaire aquifer of southern Tunisia. *Carbonates and Evaporites, 25,*
589 *65-75.*

590 **A**bid, K., Dulinski, M., Hadj Ammar, F., Rozanski, K., Zouari, K., 2011. Deciphering
591 interaction of regional aquifers in Southern Tunisia using hydrochemistry and isotopic tools.
592 *J. Appl. Geochem. 27, 44–55.*

593 **A**bid, K., Hadj Ammar, F., Chkir, N., Zouari, K., 2012. Relationship between Senonian and
594 deep aquifers in Southern Tunisia. *Quaternary International, 257, 13-26.*

595 Abid, A., Hadj Ammar, F., Weise, S., Zouari, K., Chkir, N., Rozanski, K., Osenbrück, K.,
596 2014. Geochemistry and residence time estimation of groundwater from MioceneePliocene
597 and Upper Cretaceous aquifers of Southern Tunisia Quaternary International 338 (2014) 59-
598 70.
599 **A**dam, A.A., Mohamed Ahmed, H.E., Omar, B.I., 2011. Uranium recovery from Uro area
600 phosphate ore, Nuba Mountains, Sudan. *Arabian Journal of Chemistry,*
601 *doi:10.1016/j.arabjc.2010.12.017.*

602 **A**ggarwal, K.P., Araguas, L.A., Choudhry, M., Duren, M., Froehlich, K., 2013. Lower
603 Groundwater ^{14}C Age by Atmospheric CO_2 Uptake During Sampling and Analysis.*National*
604 *GroundWater Association. doi: 10.1111/gwat.12110.*

605 **A**lloway, B.J., 2013. Chapter 26 Uranium. B.J. Alloway (Ed.), Heavy Metals in Soils,
606 *Springer (2013), p. 565.*

607 **A**ndrews J.N., Kay, R.L.F., 1978. The evolution of enhanced $^{234}U/^{238}U$ activity ratios for
608 dissolved uranium and ground-water dating. U.S. Geol. & TV. *Open File Report 78-701.*

609 **A**ndrews, J. N., Ciles, I. S., Kay, R. L. F., Lee, D. J., Osmond, J. K., Cowart, J. B., Fritz P.,
610 Barker J. F., Gale, J., 1982. Radioelements, radiogenic helium and age relationships for
611 groundwaters from the granites at Strioa. Sweden. *Ceochim. Cosmochim. Acta 46, 1533-1543.*

612 **A**ndrews, J.N., Kay, R.L.F., 1983. The U contents and $^{234}U/^{238}U$ activity ratios of dissolved
613 uranium in groundwaters from some Triassic sandstones in England. *Isotope Geosci. 1, 101–*
614 *117.*

615 **A**rendt, J. W., butz, T. R., Pritz, P. M., Berman, D. E., 1980. Hydrogeochemical and stream
616 sediment reconnaissance basic data for Alliance NTMS Quadrangle, Nebraska; Kansas Union
617 Carbide Corp, *Oak Ridge pp.3-A39.*

618 **A**riztegui, D., Asioli, A., Lowe, J.J., Trincardi, F., Vigliotti, L., Tamburini, F., Chondrogianni,
619 C., Accorsi, C.A., Bandini Mazzanti, M., Mercuri, A.M., Van der Kaars, S., McKenzie, J.A.,
620 Oldfield, F., 2000. Palaeoclimate and the formation of sapropel S1: inferences from Late
621 Quaternary lacustrine and marine sequences in the central Mediterranean region.
622 *Palaeogeography Palaeoclimatology Palaeoecology 158, 215-240.*

623 **B**aba Sy, O. 2005. Recharge et paleorecharge du Systeme Aquifere du Sahara Septentrional
624 (SASS). *Ph.D. thesis Universite Tunis El Manar.*

Beazley, M.J., Martinez, R.J., Webb, S.M., Sobecky, P.A., Taillefert, M., 2011. The effect of pH and natural microbial phosphatase activity on the speciation of uranium in subsurface soils. *Geochim. Cosmochim. Acta, 75 (19), pp. 5648-5663*.

Biely, A., Memmi, L., Salaj, J., 1972. Le Crétacé inferieur de la région d'Enfidha. Découverte d'Aptien condensé. Livre jubilaire M. Solignac. *Ann Min Géol Tunis 26:168-178*.

Bonotto, D.M., Andrews, J.N., 2000. The transfer of uranium Isotopes ^{234}U and ^{238}U to the waters interacting with carbonates from Mendip Hills area (England). *Appl. Radiat.Isot.52, 965–983*.

Bouaziz, S., 1986. The deformation in the Southern Tunisia Plateform; multiscalar and pluridisciplinar approach. *Doctorate of Sfax university. 180p.*

Bouaziz, S., 1995. Etude de la tectonique cassante dans la plateforme et l'Atlas Sahariens (Tunisie Meridionale): Evolution des paleochamps de contraintes et implications géodynamiques. *Thèse de Doctorat, Fac. Sc. De Tunis, 301p*.

Braun, K.; Nehme, C.; Pickering, R.; Rogerson, M.; Scroxton, N., 2019. A Window into Africa's Past Hydroclimates: The SISAL-v1 Database Contribution. *Quaternary, 2, 4*.

Buckau, G., Artinger, R., Fritz, P., Geyer, S., Kim, J. I., Wolf, M., 2000a. Origin and mobility of humic colloids in the Gorleben aquifer system. *Appl. Geochem. 15, 171–179*.

Burkitbayev, M., Uralbekov, B., Nazarkulova, S., Matveyeva, I., Vintró Luis, L., 2012. Uranium series radionuclides in surface waters from the Shu river (Kazakhstan). *J Environ Monit. 14, 1189-1194*.

Burollet, 1956. Contribution à l'étude stratigraphique de la Tunisie central. *Ann. Min. et Géol., N° 18, 352p., 93*.

Busson, G., 1967. Le Mésozoïque saharien. 1ère partie: L'Extrême Sud-tunisien. Edit., Paris, «Centre Rech. Zones Arides».*Géol., 8, 194 p. Ed. C.N.R.*

Busson, G., 1970. Le Mésozoïque saharien. 2ère partie. Essai de synthède des données des sondages Algéro-Tunisien. *2 tome. Ed, Paris, C.N.R.S. Géol. 11, 811p.*

Castany, G., 1954. L'accident Sud-Tunisien, son âge et ses relations avec l'accident Sud-Atlasique d'Algérie – *C.R. Séances Acad. Sc. Paris, V. 238, pp. 916-918*.

Causse, C., Ghaleb, B., Chkir, N., Zouari, K., Ben Ouezdou, H., Mamou, A., 2003. Humidity changes in southern Tunisia during the Late Pleistocene inferred from U–Th dating of mollusc shells. *Applied Geochemistry (18). 1691–1703.*

Chaâbani, F., 1995. Dynamique de la partie orientale du bassin de Gafsa au Paléogène. Etude minéralogique et géochimique de la série phosphatée Eocène, Tunisie méridionale. *Doctorat d'Etat, Université Tunis II. Tunisie. p 428*.

Chabaux, F., Riotte, J., Dequincey, O., 2003. Weathering and surface waters. *Rev. Mineral.Geochem. 52, 533-576*.

Chabaux, F., Bourdon, B., Riotte, J., 2008. U-series Geochemistry in weathering profiles, river waters and lakes. In: Krishnaswami, S., Cochran, J.K. (Eds.), U/Th Series Radionuclides in Aquatic Systems. *Radioactivity in the Environment 13, 49–104*.

Chae, G., Yun, S., Kim, K., Mayer, B., 2006. Hydrogeochemistry of sodium bicarbonate type bedrock groundwater in the Pocheon spa area, South Korea: water–rock interaction and hydrologic mixing. *J. Hydrol. 321, 326–343*.

Chalov, P. I., Tuzova, T. V., Musin YE. A., 1964. The $^{234}U/^{238}U$ ratio in natural waters and its use in nuclear geochronology. *Geochem. Int. 1, 402-408*.

Chalov, P. I., Svetlichnaya, N. A., Tuzova, T. V., 1970. Umnium-234 and umnium-238 in the waters and bottom sediments of Lake Balkhash and the age of the lake. *Geochem. Int. 7, 604-610*.

Chkir, N., Zouari, K., 2007. Uranium isotopic disequilibrium for groundwater classification: first results on complexe terminal and continental intercalaire aquifers in southern tunisia. *Environmental Geology, 53(3):677–685*.

Chkir, N., Guendouz, A., Zouari, K., Hadj Ammar, F., Moulla, A.S., 2009. Uranium isotopes in groundwater from the continental intercalaire aquifer in Algerian Tunisian Sahara (Northern Africa). *J. Environ. Radioact. 100, 649–656*.

Chkir, N., Hadj Ammar, F., Zouari, K., 2012. Naturally Occurring Uranium in Groundwater of the North Western Sahara Aquifer System (Northern Africa). *Occurrence and Human Exposure Chapters, Nova Science Publishers. pp. 147*.

Clark, I.D., Fritz, P., 1997. Environmental Isotopes in Hydrogeology. *Lewis Publishers, 328 p*.

Condon, D.J., McLean, N., Noble, S.R., Bowring, S.A., 2010. Isotopic composition ($^{238}U/^{235}U$) of some commonly used uranium reference materials, *Geochimica et Cosmochimica Acta 74, 7127–7143*.

Cumberland, S.A., Douglas, G., Grice, K., Moreau, J.W., 2016. Uranium mobility in organic matter-rich sediments: A review of geological and geochemical processes. *Earth-Science Reviews (159),160–185.*

Davis, D.W., Krogh, T.E., 2001. Preferential dissolution of ^{234}U and radiogenic Pb from α-recoil-damaged lattice sites in zircon: implications for thermal histories and Pb isotopic fractionation in the near surface environment. *Chem. Geol. 172, 41–58*.

Dhaoui, Z., Chkir, N., Zouari, K., Hadj Ammar, F., Agoune, A., 2016. Investigation of uranium geochemistry along groundwater flow path in the Continental Intercalaire aquifer (Southern Tunisia). *Journal of Environmental Radioactivity 157, 67-76*.

Durand, S., Chabaux, F., Rihs, S., Duringer, P., Elsass, P. 2005. U isotope ratios as tracers of groundwater inputs into surface waters: Example of the Upper Rhine hydrosystem. *Chemical Geology 220. 1-19.*

Edmunds, W.M., Shand, P., Guendouz, A.H., Moulla, A.S., Mamou, A., Zouari, K., 1997. Recharge Characteristics and Groundwater Quality of the Grand Erg Orientale Basin. *British Geological Survey*.

Edmunds, W.M., Guendouz, A.H., Mamou, A., Moulla ,A.S., Shand, P., Zouari, K., 2003. Groundwater evolution in the Continental Intercalaire aquifer of southern Algeria and Tunisia: traceelement and isotopic indicators. *Appl Geochem 18(6), 805–822*.

Edmunds, W.M., Dodo, A., Djoret, D., Gaye, C.H., Goni, I.B., Travi, Y., Zouari, K., Zuppi, G., Gasse, F., 2004. Groundwater as an archive of climatic and environmental change: Europe to Africa. Past climate variability through Europe and Africa. *Dev. Paleoenviron. Res. 6, 279–306*.

Eichinger, L., 1983. A contribution to the interpretation of 14C groundwater ages considering the example of a of a partially confined sandstone aquifer.*Radiocarbon, 25, 347-356*.

710 **E**lliot, T., Bonotto, D. M., Andrews, J. N., 2014. Dissolved uranium, radium and radon
711 evolution in the Continental Intercalaire aquifer, Algeria and Tunisia. *Journal of*
712 *Environmental Radioactivity, 137, 150-162*.

713 **E**RESS, 1972. Etude des Ressources en Eau de Sahara Septentrional. *UNESCO, Paris, vol. 7*
714 *et annexes*.

715 **E**scorcia, L.C., Gomez-Rivas, E., Daniele, L., Corbella, M., 2013. Dedolomitization and
716 reservoir quality: insights from reactive transport modelling. *Geofluids 13, 221–231.*

717 **E**ssallami, L., Sicre, M.A, Kallel, N., Labeyrie, L., Siani, G., 2007. Hydrological changes in
718 the Mediterranean Sea over the last 30,000 years. *Geochem. Geophys. Geosyst.,8, Q07002,*
719 *doi:10.1029/2007GC001587.*

720 **E**vans, G.V, Otlet, R.L., Downing, A., Monkhouse, R.A., Rae, G., 1979. Some problems
721 interpretation of isotope measurements in United Kingdom Aquifers. *Isotopes in Hydrology*
722 *II, IAEA, Vienna*.

723 **F**ontes, J., Garnier, J., 1979. Determination of the initial ^{14}C activity of the total dissolved
724 carbon: A review of the existing models and a new approach. *Water Resources Research, 15,*
725 *399-413*.

726 **F**ontugne, M., Arnold, M., Labeylie, L., Patern, M., Calvert, S.E., Duplessy, J.E., 1994.
727 Paleoevirement sapropel chronology and Nile river discharge during the last 20,000 years as
728 indicated by deep-sea sediment records in the eastern Mediterranean. Late Quaternary
729 Chronology and Paleoclimat of the Eastern Mediterranean. *Radiocarbon, 75-88*.

730 **F**rohlich, K., Gellermann, R., 1987. On the potential use of uranium isotopes for groundwater
731 dating. *Chem. Geol. 65, 67-77*.

732 **F**rohlich, K., 2013. Dating of old groundwater using uranium isotopes d Principles and
733 applications. In: Isotope Methods for Dating Old Groundwater. *International Atomic Energy*
734 *Agency, Vienna, pp. 153-178.*

735 **G**allala, W., Saïdi, M., el Hajii, S., Zayani, K., Essghaier Gaied, M., Montacer, M., 2016.
736 Characterization and Valorization of Tozeur-Nefta Phosphate Ore Deposit (Southwestern
737 Tunisia). *Procedia Engineering, 138, 8 – 18*.

738 **G**ascoyne, M., 1992. Geochemistry of the actinides and their daughters. In: Ivanovich, M.,
739 Harmon, R.S. (Eds.), Uranium- Series Disequilibrium: Applications to Earth, Marine, and
740 Environmental Sciences 2nd Edition. *Clarendon Press, Oxford, pp. 34–61*.

741 **G**enty, D., Blamart, D., Ouahdi, R., Gilmour, M., Baker, A., Jouzel, J., Van-Exter, S., 2003.
742 Precise dating of Dansgaard–Oeschger climate oscillations in Western Europe from
743 stalagmite data. *Nature 421(6925):833-7. DOI: 10.1038/nature01391.*

744 **G**enty, D., Blamart, D., Ghaleb, B., Plagnes, V., Causse, C.h., Bakalowicz, M., Zouari, K.,
745 Chkir, N., Hellstrom, J., Wainer, K., and Bourges, F., 2006. Timing and dynamics of the last
746 deglaciation from European and North African $\delta^{13}C$ stalagmite profiles comparison with
747 Chinese and South Hemisphere stalagmites. *Quaternary Sci. Rev., 25, 2118–2142.*

748 **G**eyh, M.A., 2000. An overview of ^{14}C analysis in the study of groundwater. *Radiocarbon,*
749 *42, 99–114*.

750 **G**eyh, M.A., 2005. Dating of old groundwater - History, potential, limits and future, in: P.K.
751 Aggarwal, Gat, J.R. Froehlich, K.F.O. (eds.), Isotopes in the Water Cycle, Past, Present and
752 Future of a Developing Science. *Springer, The Netherlands, pp. 221–241*.

753 **G**oncalves, J., Petersen, J., Deschamps, P., Hamelin, B., BabaSy, O., 2013. Quantifying the
754 modern recharge of the "fossil" Sahara aquifers. *Geophysical Research Letters, 40, 1-6*.

755 **G**uendouz, A., Moulla, A.S., Edmunds, W.M., Shand, P., Zouari, K., Mamou, A., 1997.
756 Palaeoclimatic information contained in groundwaters of the Grand Erg Oriental, North
757 Africa. In: *Int. Symp. Isotope Techniques in the Study of Past and Current Environmental*
758 *Changes in the Hydrosphere and Atmosphere, Vienna, IAEA, pp. 555–571*.

759 **G**uendouz, A., Moulla, S., Edmunds, W. M., Zouari, K., Shand, P., Mamou, A., 2003.
760 Hydrogeochemical and isotopic evolution of water in the Complexe Terminal aquifer in the
761 Algerian Sahara. *Hydrogeology Journal, 11, 483–495*.

762 **H**adj Ammar, F., Chkir, N., Zouari, K., Azzouz-Berriche, Z., 2010. Uranium isotopes in
763 groundwater from the "Jeffara coastal aquifer" (southeastern Tunisia). *Journal of*
764 *Environmental Radioactivity 101, 681-691*.

765 **H**adj Ammar, F., Chkir, N., Zouari, K., Hamelin, B., Deschamps, P., Aigoun, A., 2014.
766 Hydro-geochemical processes in the Complexe Terminal aquifer of southern Tunisia: An

integrated investigation based on geochemical and multivariate statistical methods. *Journal of African Earth Sciences (100) 81–95*.

Hadj Ammar, F., 2016. Caractérisation des eaux de l'Aquifère du Complexe Terminal: Approche multi-isotopiques ($^{234}U/^{238}U$, ^{36}Cl, ^{14}C, $\delta^{18}O$, $\delta^{2}H$)». *Université de Sfax/Aix-Marseille Université, Thèse Doctorat. p 230.*

Han, L.F., Plummer, L.N., 2013. Revision of Fontes & Garnier's model for the initial ^{14}C content of dissolved inorganic carbon used in groundwater dating. *Chem. Geol., 351, 105–114*.

Han, L.F., Plummer, L.N., 2016. A review of single-sample-based models and other approaches for radiocarbon dating of dissolved inorganic carbon in groundwater.*Earth Science Reviews, doi: 10.1016/j.earscirev.2015.11.004.*

Hiscock, K.M., 2005. Hydrogeology: Principles and Practice, first ed. Blackwell Publishing, *Oxford, Hiscock, pp. 406*.

Ingerson, E., Pearson, F. J., 1964. Estimation of age and rate of motion of ground water by the carbon-14 method, in: *Koyama, Tadashiro (ed.),Mazuren, Toyko, Recent researches in the fields of hydrosphere, atmosphere, and nuclear geochemistry, p. 263-283*.

Ivanovich, M., Frohlich, K., Hendry, M.J., 1991. Uranium-series radionuclides in fluids and solids from the Milk River aquifer, Alberta, Canada. Appl. Geochem 6, 405-418.

Ivanovitch, M., Harmon, R.S., 1992. Uranium series disequilibrium. *Clarendon press, Oxford*.

Jarraya, H., Hadj Ammar, F., Abid, K., Zouari, K., Aissa, A., 2013. Study of Rejim Maatoug groundwater in southern Tunisia using isotope methods. *Journal of Hydro-environment Research. Volume 8, Issue 3, 316-327*.

Kallel, N., Duplessy, J.-C., Labeyrie, L., Fontugne, M., Paterne, M., Montacer, M., 2000. Mediterranean pluvial periods and sapropel formation over the last 200000 years. *Palaeogeography Palaeoclimatology Palaeoecology 157, 45-58*.

Kamel, S., 2007. Caractérisation hydrodynamique et géochimique des aquifères du Djérid (Sud Tunisien). *Université de Tunis, Thèse Doctorat. p 230*.

Kamel, S., Hamed, Y., Chkir, N., Zouari, K., 2007. The hydro geochemical characterization of ground waters in Tunisian Chott's region. *Environ. Geol. J. 54, 843–854*.

Kronfeld, J. Adams, J. A. S., 1974. Hydrologic investigations of the groundwaters of central Texas using $^{234}U/^{238}U$ disequilibrium. *J. HyroI. 22, 77-88*.

Kronfeld, J., Vogel, J.C., Talma, A.S., 1994. A new explanation for extreme $^{234}U/^{238}U$ disequilibria in a dolomitic aquifer. *Earth Planet. Sci. Let. 123, 81–93*.

Langmuir, D., 1978. Uranium solution e mineral equilibria at low temperatures with applications to sedimentary ore deposits. *Geochim. Cosmochim. Acta 42, 547-569*.

Luo, W., Gao, X., Zhang, X., 2018. Geochemical processes controlling the groundwater chemistry and fluoride contamination in the Yuncheng Basin, China—An area with complex hydrogeochemical conditions. PLoS ONE 13(7): e0199082. https://doi.org/10.1371/journal pone.0199082.

Maher, K., Steefel, C.I., DePaolo, D.J., Viani, B.E., 2006. The mineral dissolution rate conundrum: insights from reactive transport modeling of U isotopes and pore fluid chemistry in marine sediments. *Geochim. Cosmochim. Acta 70, 337-363*.

Malov, A.I., 2013. Application of geological benchmarks for determining groundwater residence time in the aquifer based on uranium isotope data: evidence from the Severnaya Dvina Basin. *Lithol. Min. Resour. 48 (3), 254-265*.

Malov, A.I., 2016. Estimation of uranium migration parameters in sandstone aquifers. *Journal of Environmental Radioactivity 153. 61-67*.

Mamou, A., 1990. Caractéristiques, Evaluation, Gestion des Ressources en eau du Sud Tunisien. *Thèse de Doctorat, Es Science, Université Paris Sud, pp. 426*.

Mannai-Tayech, B., 2009. The lithostratigraphy of Miocene series from Tunisia. *Afr. Earth Sci. J. 54, 53–61 (revisited).*

McKelvey, V.E., Everhart, D.L., Garrels, R.M., 1955. Origin of uranium deposits. *Economic Geology (50th Anniversary Volume), 464–533*.

Mehta, V.S., Maillot, F., Wang, Z., Catalano, J.G., Giammar, D.E., 2014. Effect of co-solutes on the products and solubility of uranium(VI) precipitated with phosphate. *Chem. Geol., 364 (0), pp. 66-75.*

Mejean, P., Pinti, D.L., Larocque, M., Ghaleb, B., Meyzonnat, G., Gagn, S., 2016. Processes controlling 234U and 238U isotope fractionation and helium in the groundwater of the St. Lawrence Lowlands, Quebec: The potential role of natural rock fracturing. *Applied Geochemistry (66). 198-209.*

Moulla, A., Guendouz, A., Cherchali, M.-H., Chaid, Z., and Ouarezki, S., 2012. Updated geochemical and isotopic data from the Continental Intercalaire aquifer in the Great Occidental Erg sub basin (south-western Algeria).*Quatern. Int., 257, 64–73*.

Osmond, J.K., Kaufman, M.I., Cowart, J.B., 1974. Mixing volume calculations, sources and aging trends of Floridan aquifer water by uranium isotopic methods. *Geochim. Cosmochim. Acta (38), 1083-1100.*

Osmond, J.K., Cowart, J.B., 1976. The theory and uses of natural uranium isotopic variations in hydrology. *At. Energy Rev. 14, 621-679*.

Osmond, J.K., Ivanovich, M., 1992. Uranium-Series mobilization and surface hydrology. In: Ivanovich, M., Harmon, R.S. (Eds.), Uranium-Series Disequilibrium. *Clarendon Press, Oxford, 259-289*.

Osmond, J.K., Cowart, J.B., 2000. U-series nuclides as tracers in groundwater hydrology. In: Environmental tracers in subsurface hydrology (Eds P. Cook and A. Herczeg). *Kluwer Academic Publishers, Boston, pp. 290–333*.

OSS, 2003. Système Aquifère du Sahara Septentrional. In: *Hydrogéologie, vol. 2. OSS, Tunis Int. Rep. Project SASS.*

Paces, J.B., Ludwig, K.R., Peterman, Z.E., Neymark, L.A., 2002. $^{234}U/^{238}U$ evidence for local recharge and patterns of ground-water flow in the vicinity of Yucca Mountain, Nevada, USA. *Appl. Geochem 17, 751-779*.

Paces, J.B., Wurster, F.C., 2014. Natural uranium and strontium isotope tracers of water sources and surface water-groundwater interactions in arid wetlands-Pahranagat Valley, Nevada, USA. *J. Hydrol. 517, 213-225.*

Pearson, F. J., Noronha, C. J. and Andrews, R. W., (1983). Mathematical modelling of the distribution of natural ^{14}C, ^{234}U and ^{238}U in a regional groundwater system. *Radiocarbon 25, 291-300*.

Penna, D., Stenni, B., Sanda, M., Wrede, S., Bogaard, T. A., Gobbi, A., Borga, M., Fischer, B. M. C., Bonazza, M., Charova, Z., 2010. On the reproducibility and repeatability of laser absorption spectroscopy measurements for δ^2H and $\delta^{18}O$ isotopic analysis. *Hydrol. Earth Syst. Sci., 14, 1551–1566*.

Petersen, J. O., Deschamps, P., Hamelin, B., Goncalves, J., Michelot, J.L., Zouari, K., 2013. Water-rock interaction and residence time of groundwater inferred by $^{234}U/^{238}U$ disequilibria in the Tunisian Continental Intercalaire aquifer system. *Procedia Earth and Planetary Science,7, 685-688*.

Petersen, J. O., Deschamps, P., Goncalves, J., Hamelin, B., Michelot, J. L., Guendouz, A., Zouari, K., 2014. Quantifying paleorecharge in the Continental Intercalaire (CI) aquifer by a Monte-Carlo inversion approach of data. *Applied Geochemistry, 50, 209-221*.

Petersen, J.O., Deschamps, P, Hamelin, B., Fourré, E., Gonçalvès, J. Zouari, K., Guendouz, A., Michelot, J.-L., Massault, M., Dapoigny, A., Aster Team., 2018. Groundwater flowpaths and residence times inferred by ^{14}C, ^{36}Cl and ^{4}He isotopes in the Continental Intercalaire aquifer (North-Western Africa). *J. Hydrol. doi: https://doi.org/10.1016/j.jhydrol.2018.03.003*.

Porcelli, D., Swarzenski, P.W., 2003. The behavior of U- and Th-series nuclides in ground water. In: Bourdon, B., Henderson, G.M., Lundstrom, C.C., Turner, S.P. (Eds.), Uranium-Series Geochemistry. *Rev. Mineral. Geochem. 52, 317–361*.

Riedel, Th., Kübeck, Ch., 2018. Uranium in groundwater- A synopsis based on a large hydrogeochemical data set. *Water Research 129. 29-38.*

Riotte, J., Chabaux, F., 1999. ($^{234}U/^{238}U$) activity ratios in freshwaters as tracers of hydrological processes: the Strengbach watershed (Vosges, France). Geochim. Cosmochim. Acta 63, 1263-1275.

Riotte, J., Chabaux, F., Benedetti, M., Dia, A., Gerard, M., Boulegue, J., 2003. U colloidal transport and origin of the $^{234}U–^{238}U$ fractionation in surface waters: new insights from Mount Cameroon. *Chem. Geol. 202, 365– 381*.

879 **S**alem, O., Visser, J.H., Dray, M., Gonfiantini, R., 1980. Environmental isotopes used in a
880 hydrogeological study of north-eastern Brazil, Arid zone Hydrology: Investigations with
881 isotope Techniques.*Panel Proceedings Series No, 134,IAEA, Vienna*.

882 **S**andino, A., Bruno, J., 1992. The solubility of $(UO_2)_3(PO_4)_2.4H_2O(s)$ and the formation of
883 U(VI) phosphate complexes: their influence in uranium speciation in natural waters. *Geochim.*
884 *Cosmochim. Acta, 56 (12), pp. 4135-4145.*

885 **S**chipper, L.A., Sparling, G.P., Fisk, L.M., Dodd, M.B., Power, I.L., Littler, R.A., 2011. Rates
886 of accumulation of cadmium and uranium in a New Zealand hill farm soil as a result of long-
887 term use of phosphate fertilizer Agric. *Ecosyst. Environ., 144 (1), pp. 95-101.*

888 **S**assi, S., 1974. La sédimentation phosphatée au Paléocène dans le Sud et le centre Ouest de
889 la Tunisie.*Thèse de Doctorat és-Sciences, Université de Paris Sud Orsay, 292 p*.

890 **S**medley, P.L., Smith, B., Abesser, C., Lapworth, D., 2006. Uranium occurrence and
891 behaviour in British groundwater. *British Geological Survey Commissioned Report,*
892 *CR/06/050N. 60 p*.

893 **S**palding, R. F., Druliner, A. D., 1981. Groundwater uranium concentrations-How high is
894 high? *In Quality of Groundwater (eds. W. VAN DUIJVENBOODEN, P. GLASBERGEN and*
895 *H. VAN LELYVELD), pp. 581-586*.

896 **S**tuiver, M., Polach, H.A., 1977. Discussion: Reporting of ^{14}C Data. *Radiocarbon 19(3), 355-*
897 *363*.

898 **S**tute, M., Schlosser, P., 1993. Principles and applications of the noble gas paleothermometer,
899 in: Swart, P.K., Lohmann, K.C., McKenzie, J., Savin, S. (Eds.), Climate change in continental
900 isotopic records. *AGU, Washington DC, pp. 89-100*.

901 **T**lig, S., Erraioui, L., Ben Aissa, L., Aluoani, R., Tagorti, M.A., 1991. Tectogenèses alpine et
902 atlasique: deux événements distincts dans l'histoire géologique de la Tunisie. Corrélation avec
903 les événements clés en Méditerranée. *Comptes Rend. Acad. Sci. Paris 312 (Série II), pp. 295–*
904 *301*.

905 **Y**angui, H., Abidi, I., Zouari, K., Rozanski, K., 2012. Deciphering groundwater flow between
906 the Complex Terminal and Plio-Quaternary aquifers in Chott Gharsa plain (southwestern

907 Tunisia) using isotopic and chemical tools. *Hydrological Sciences Journal, 57:5, 967-984,*
908 *DOI: 10.1080/02626667.2012.689110.*

909 **Z**ammouri, M., Siegfried, S., El-Fahem, T., Kriâa, S., Kinzelbach, W., 2007. Salinization of
910 groundwater in the Nefzawa oases region, Tunisia: results of a regional-scale hydrogeologic
911 approach. *Hydrogeol. J. 15, 1357–1375*.

912 **Z**argouni, F., Rabia, M.C.H., Abbès, C.H., 1985. Rôle des couloirs de cisaillement de Gafsa et
913 de Négrine-Tozeur dans la structuration du faisceau des plis des chotts, élément de l'accident
914 Sud-Atlasique. *C. R. Acad. Sci. 301, 831–834*.

915 **Z**hu, C., Murphy, W.M., 2000. On radiocarbon dating of ground water. *Ground water, 38,*
916 *802–804*.

917 **Z**ouaghi, T., Bedir, M., Inoubli, M.H., 2005. 2D seismic interpretation of strike-slip faulting,
918 salt tectonics, and Cretaceous unconformities, Atlas Mountains, central Tunisia. *J. Afr. Earth*
919 *Sci. 43 (4), 464–486*.

920

921

922

923

924

925

926

927

928

929

930 **Figure captions**

931 **Fig.1** Simplified map of the study area, showing sample location and groundwater
932 piezometric level of the CT aquifers.

933 **Fig.2** Block diagrams illustrating the compartmentalization of the different layers of the
934 intermediate CT aquifer in both Nefzaoua (a) and Djerid (b) basins with geological groups
935 and clarifying the probable mixture with the other shallow and deeper fractured aquifers.

936 **Fig.3** The $^{234}U/^{238}U$ activity ratio (AR) and the reciprocal of the U- concentration (in ppb^{-1}) in
937 the CT groundwaters (numbers correspond to the sample identification – Table 2).

938 **Fig.4** Conceptual hydrochemical cross-sections along the generalized flow path in Nefzaoua
939 (a) and Djerid (b) basins, showing some of the main U and major ions-results.

940 **Fig.5** Plots of ^{14}C activities versus $\delta^{13}C$. The small symbols indicate the A_0 initial values
941 calculated for each point with the Fontes and Garnier (1979) model. γ This work , na: not available,
942 * Abid et al., 2011, ί Yangui et al., 2012, ε Abid et al., 2012, **Θ** Hadj Ammar et al., 2014.

943 **Fig. 6** Frequency histogram of ^{14}C model ages calculated from Fontes and Garnier (1979).

944 **Fig. 7** Spatial distribution of U- concentration.

945 **Fig. 8** Major ion contents Versus U- concentration. **Θ** Hadj Ammar et al., 2014, γ This work

946 **Fig.9** Plots of $\delta^{18}O$ content versus U- concentration. **Θ** Hadj Ammar et al., 2014, γ This work

947 **Fig.10** Spatial distribution of the main recharge periods of the CT groundwater.

948 **Tables**

949 **Table 1.** Field parameters and chemical results of analyzed groundwater samples of the CT
950 aquifer in Chott Region.

951 **Table 2.** Uranium isotopic data together with stable isotopes and ^{14}C corrected age of
952 analyzed groundwater samples of the CT aquifer.

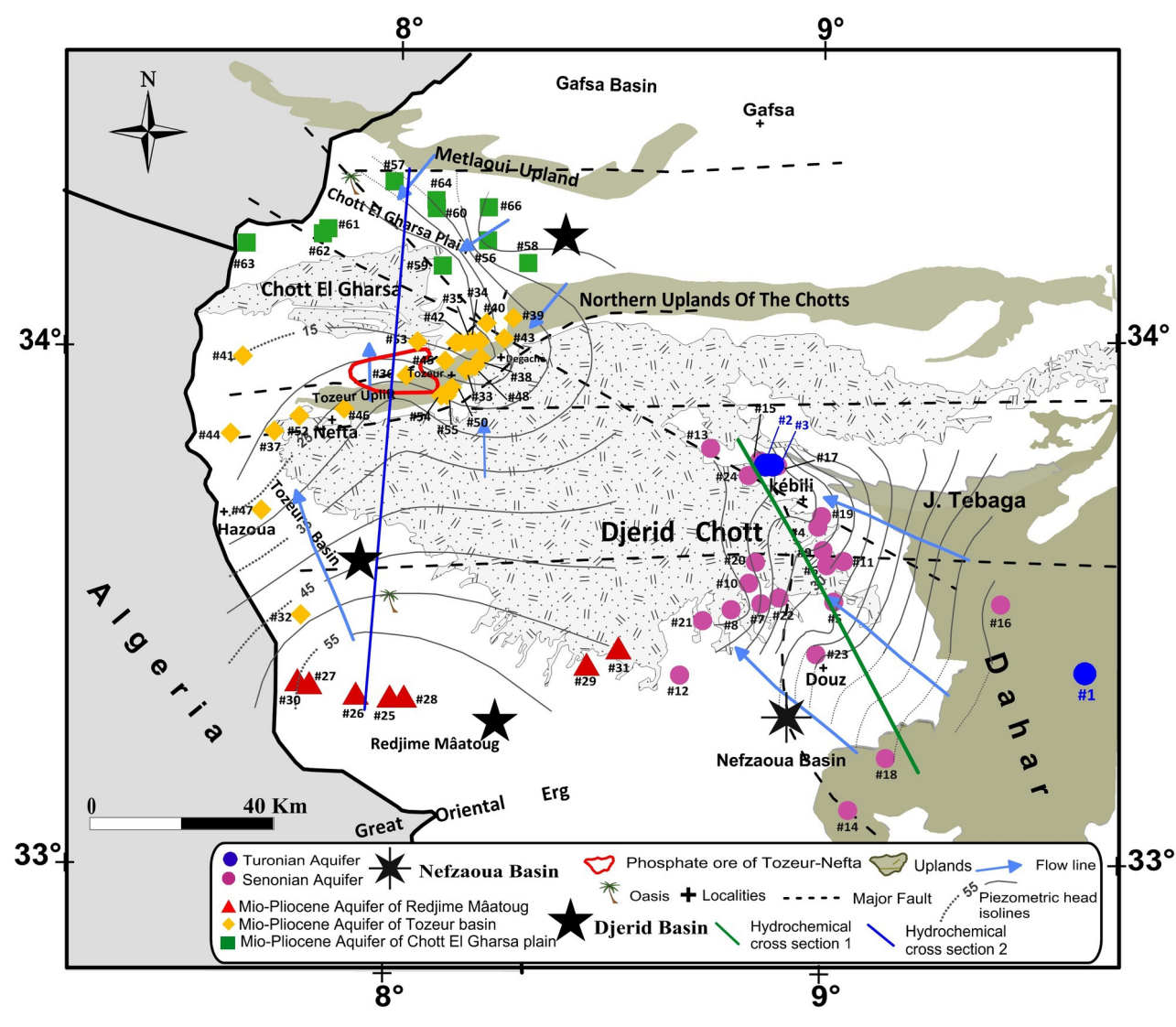
8°
9°
34°
33°
N
Gafsa Basin
Gafsa
Metlaoui-Upland
Chott El Gharsa Plai
Chott El Gharsa
Northern Uplands Of The Chotts
Tozeur Upland
Nefta
Hazoua
Tozeur Basin
Djerid Chott
kébili
J. Tebaga
Douz
Dahar
Algeria
Redjime Mâatoug
Nefzaoua Basin
Great Oriental Erg
0 40 Km
Turonian Aquifer
Senonian Aquifer
Nefzaoua Basin
Phosphate ore of Tozeur-Nefta
Uplands
Flow line
Oasis
Localities
Major Fault
Piezometric head isolines
Mio-Pliocene Aquifer of Redjime Mâatoug
Mio-Pliocene Aquifer of Tozeur basin
Mio-Pliocene Aquifer of Chott El Gharsa plain
Djerid Basin
Hydrochemical cross section 1
Hydrochemical cross section 2

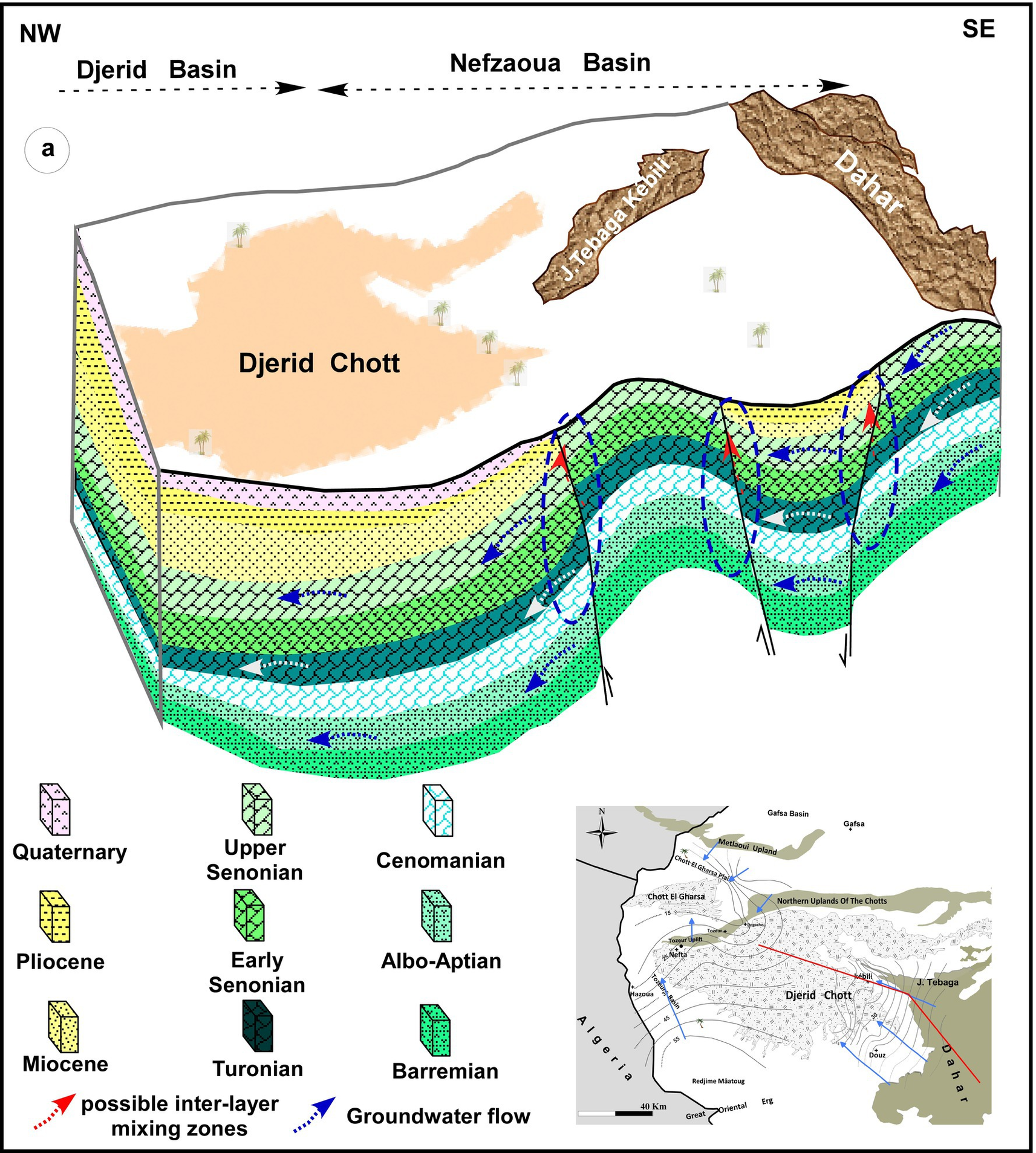
NW
SE
Djerid Basin
Nefzaoua Basin
a
J. Tebaga Kébili
Dahar
Djerid Chott
Quaternary
Upper Senonian
Cenomanian
Pliocene
Early Senonian
Albo-Aptian
Miocene
Turonian
Barremian
possible inter-layer mixing zones
Groundwater flow
N
Gafsa Basin
Gafsa
Metlaoui Upland
Chott El Gharsa Plain
Chott El Gharsa
Northern Uplands Of The Chotts
Tozaur
Tozaur Uplift
Nefta
Kébili
J. Tebaga
Hazoua
Djerid Chott
Douz
Dahar
Algeria
Redjime Mâatoug
40 Km
Great Oriental Erg

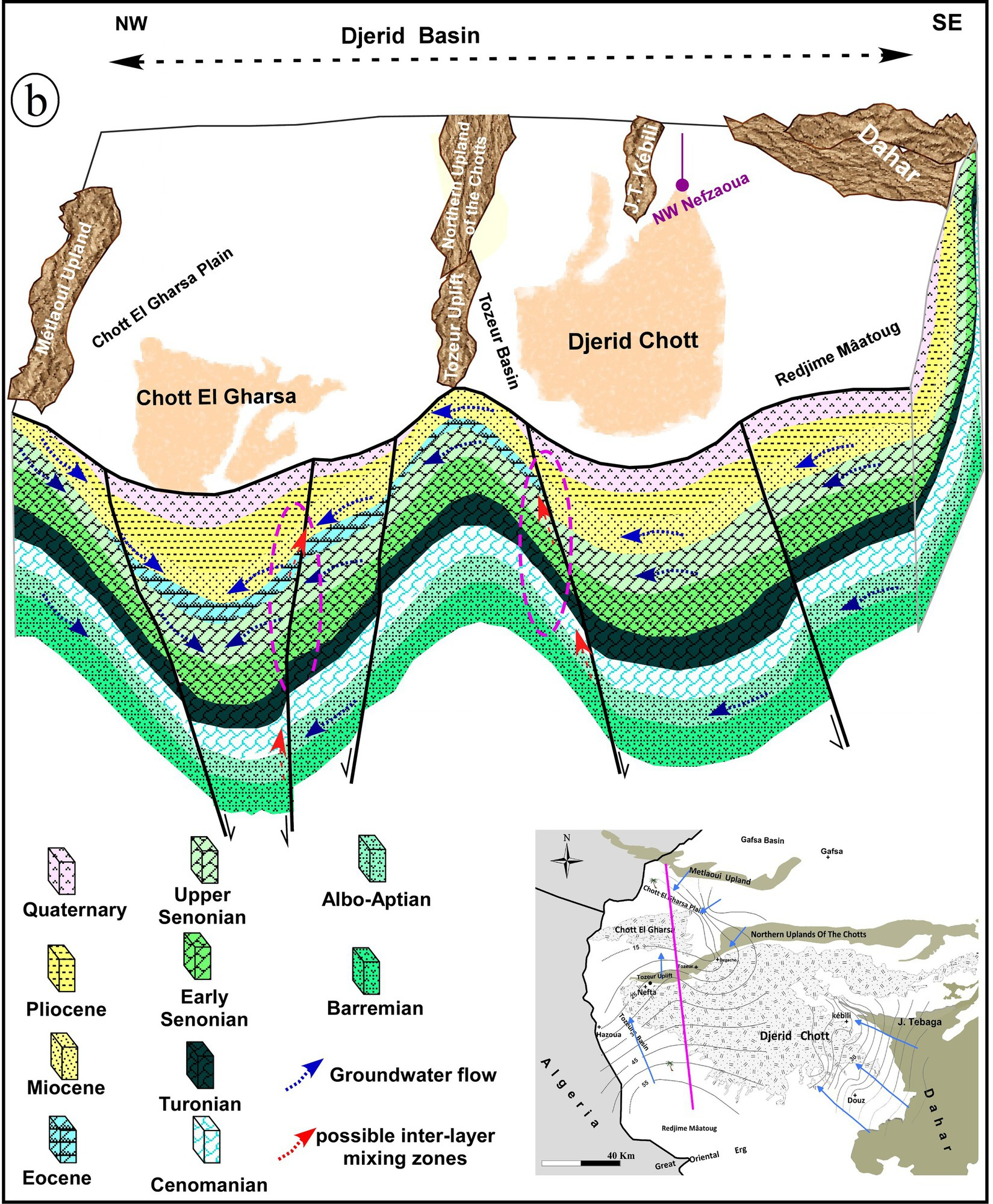
NW
Djerid Basin
SE
b
Métlaoui Upland
Chott El Gharsa Plain
Chott El Gharsa
Northern Upland of the Chotts
Tozeur Uplift
Tozeur Basin
Djerid Chott
J.T. Kébili
NW Nefzaoua
Dahar
Redjime Mâatoug
Quaternary
Pliocene
Miocene
Eocene
Upper Senonian
Early Senonian
Turonian
Cenomanian
Albo-Aptian
Barremian
Groundwater flow
possible inter-layer mixing zones
N
Gafsa Basin
Gafsa
Metlaoui Upland
Chott-El-Gharsa Plain
Chott El Gharsa
Northern Uplands Of The Chotts
Tozeur
Tozeur Uplift
Nefta
Hazoua
Tozeur Basin
Djerid Chott
kébili
J. Tebaga
Douz
Dahar
Algeria
Redjime Mâatoug
40 Km
Great
Oriental
Erg

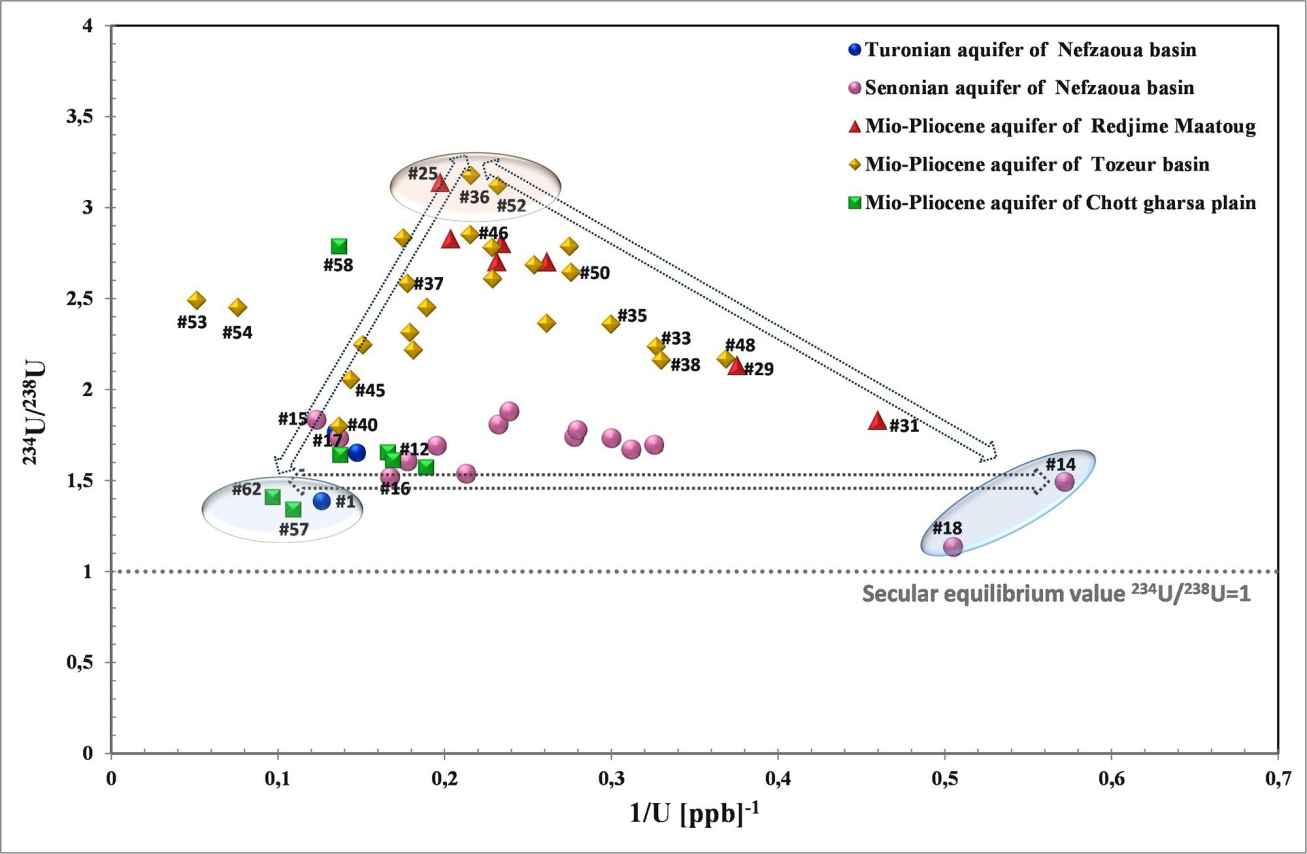
Turonian aquifer of Nefzaoua basin
Senonian aquifer of Nefzaoua basin
Mio-Pliocene aquifer of Redjime Maatoug
Mio-Pliocene aquifer of Tozeur basin
Mio-Pliocene aquifer of Chott gharsa plain
Secular equilibrium value 234U/238U=1
234U/238U
1/U [ppb]-1
#1
#12
#14
#15
#16
#17
#18
#25
#29
#31
#33
#35
#36
#37
#38
#40
#45
#46
#48
#50
#52
#53
#54
#57
#58
#62

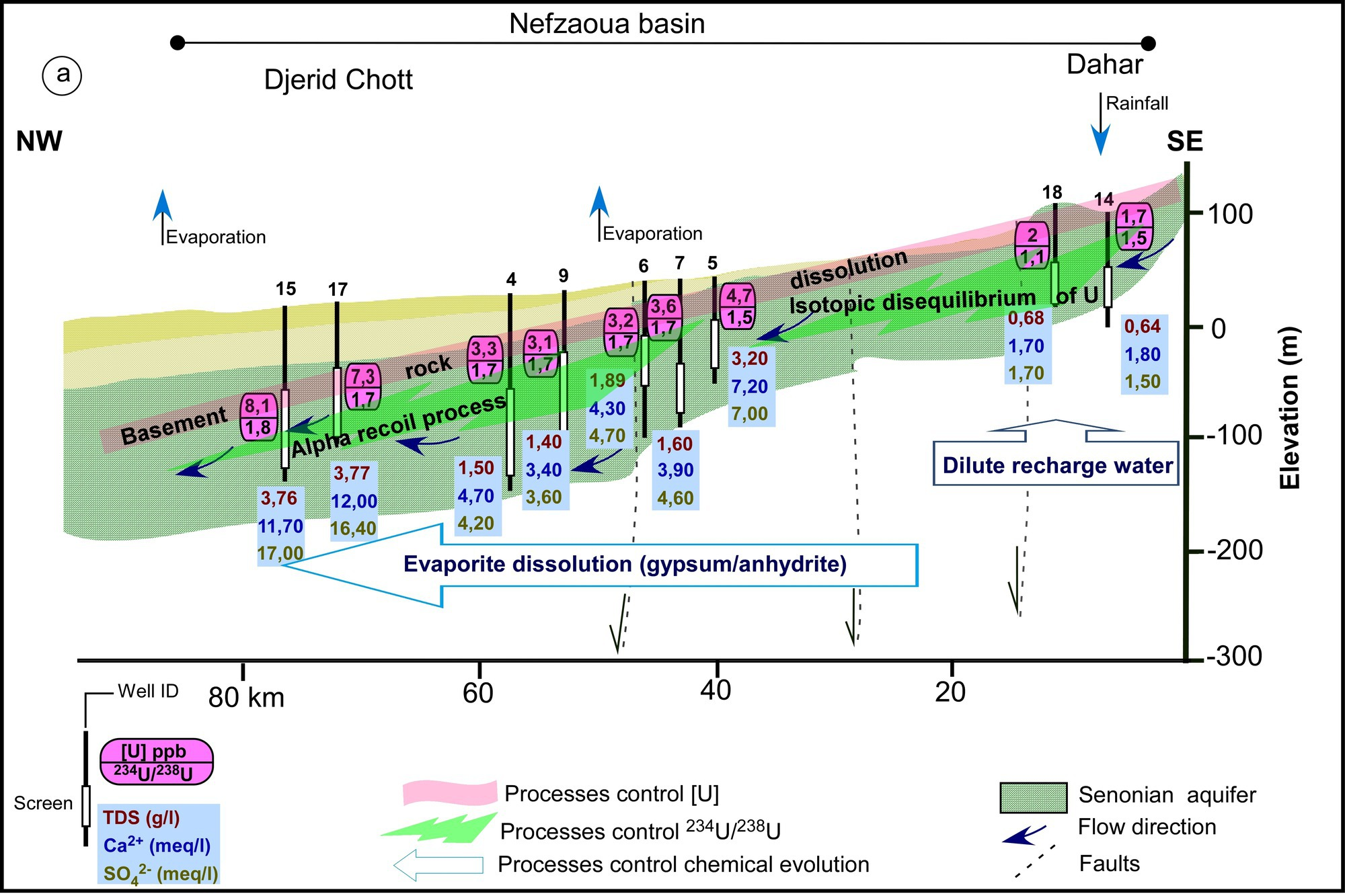
Nefzaoua basin
a
Djerid Chott
Dahar
Rainfall
NW
SE
Evaporation
Evaporation
15
17
4
9
6
7
5
18
14
dissolution
Isotopic disequilibrium of U
rock
Basement
Alpha recoil process
8,1
1,8
7,3
1,7
3,3
1,7
3,1
1,7
3,2
1,7
3,6
1,7
4,7
1,5
2
1,1
1,7
1,5
3,76
11,70
17,00
3,77
12,00
16,40
1,50
4,70
4,20
1,40
3,40
3,60
1,89
4,30
4,70
1,60
3,90
4,60
3,20
7,20
7,00
0,68
1,70
1,70
0,64
1,80
1,50
Dilute recharge water
Evaporite dissolution (gypsum/anhydrite)
100
0
-100
-200
-300
Elevation (m)
80 km
60
40
20
Well ID
[U] ppb
234U/238U
Screen
TDS (g/l)
Ca2+ (meq/l)
SO4 2- (meq/l)
Processes control [U]
Processes control 234U/238U
Processes control chemical evolution
Senonian aquifer
Flow direction
Faults

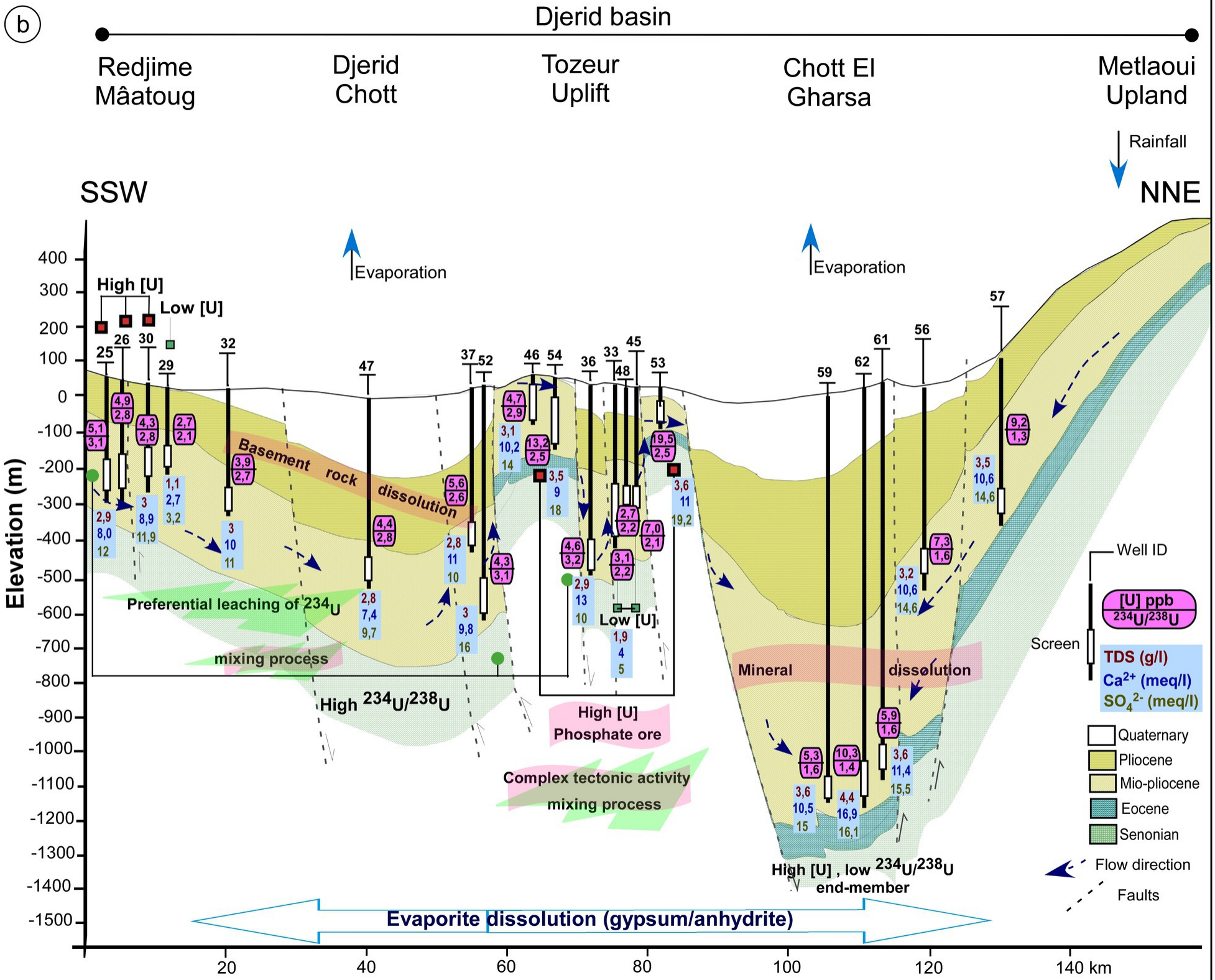
b
Djerid basin
Redjime Mâatoug
Djerid Chott
Tozeur Uplift
Chott El Gharsa
Metlaoui Upland
Rainfall
SSW
NNE
Evaporation
Evaporation
High [U]
Low [U]
Basement rock dissolution
Preferential leaching of 234U
mixing process
High 234U/238U
High [U] Phosphate ore
Low [U]
Complex tectonic activity
mixing process
Mineral dissolution
High [U] , low 234U/238U end-member
Evaporite dissolution (gypsum/anhydrite)
Elevation (m)
Well ID
[U] ppb
234U/238U
Screen
TDS (g/l)
Ca2+ (meq/l)
SO4 2- (meq/l)
Quaternary
Pliocene
Mio-pliocene
Eocene
Senonian
Flow direction
Faults
20
40
60
80
100
120
140 km

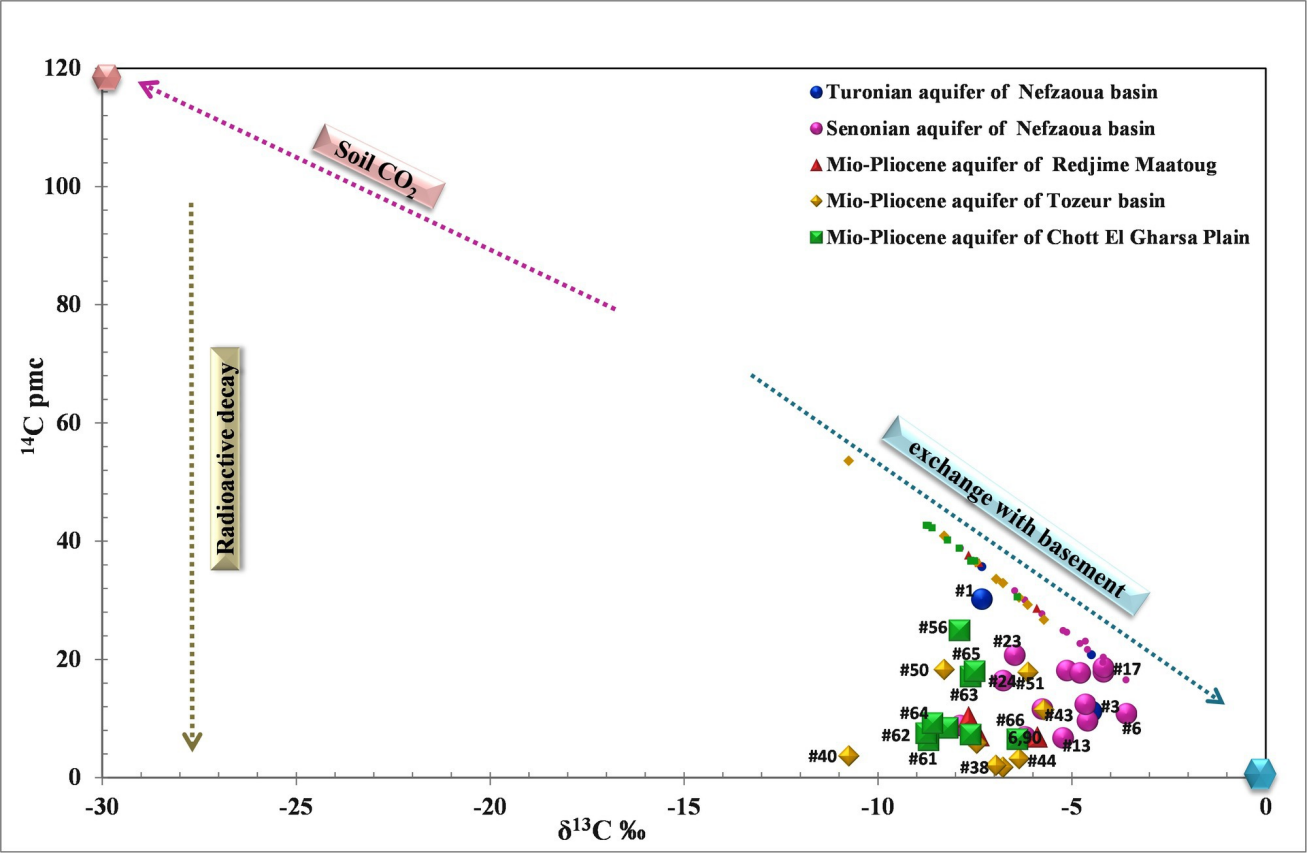
Turonian aquifer of Nefzaoua basin
Senonian aquifer of Nefzaoua basin
Mio-Pliocene aquifer of Redjime Maatoug
Mio-Pliocene aquifer of Tozeur basin
Mio-Pliocene aquifer of Chott El Gharsa Plain
Soil CO2
Radioactive decay
exchange with basement
14C pmc
δ13C ‰
120
100
80
60
40
20
0
-30
-25
-20
-15
-10
-5
0
#1
#56
#23
#65
#50
#24
#51
#17
#63
#3
#64
#43
#66
#6
#62
#13
#61
#38
#44
#40

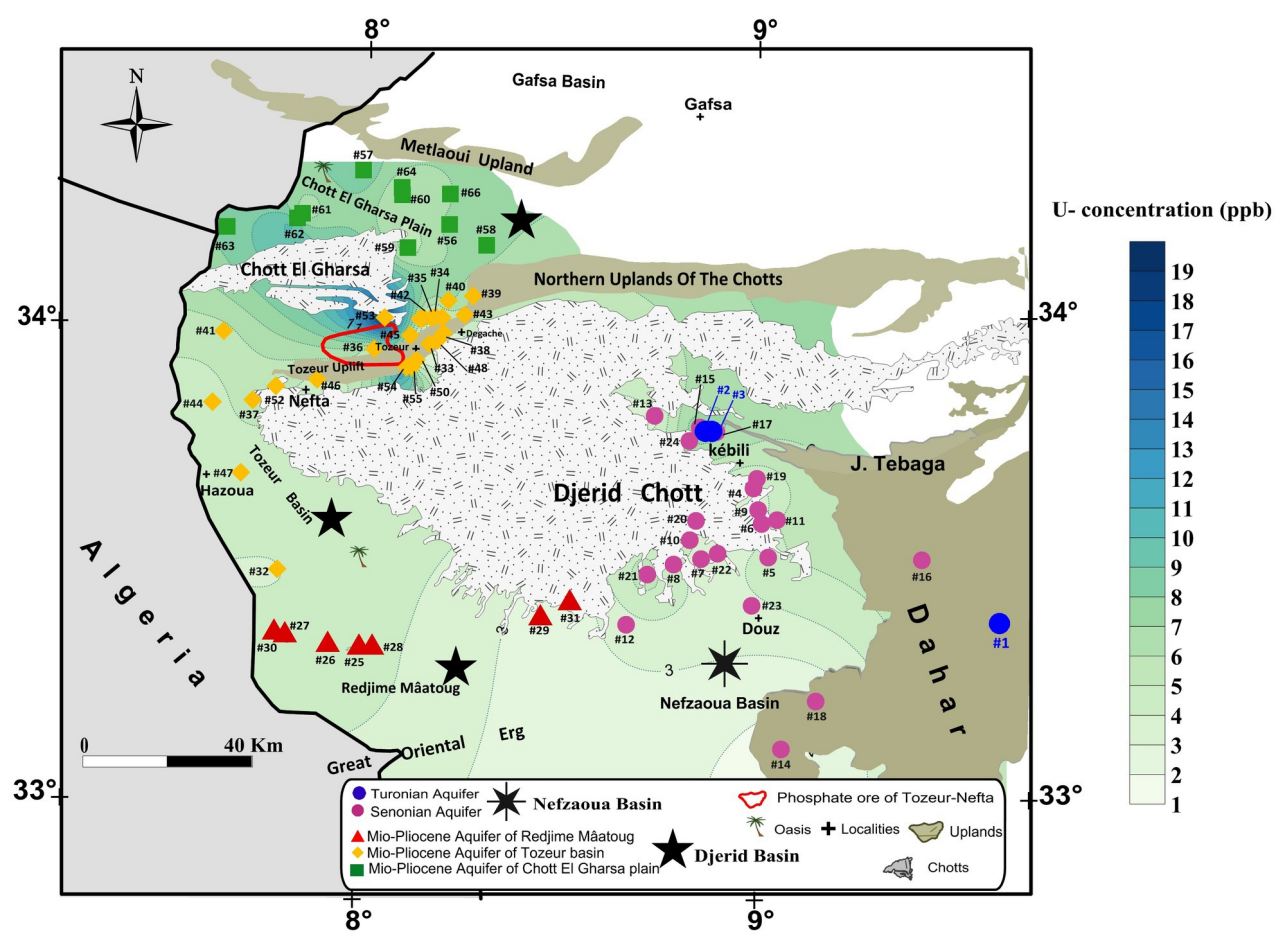
8°
9°
34°
33°
N
Gafsa Basin
Gafsa
Metlaoui Upland
Chott El Gharsa Plain
Chott El Gharsa
Northern Uplands Of The Chotts
Degache
Tozeur
Tozeur Uplift
Nefta
Hazoua
Tozeur Basin
kébili
J. Tebaga
Djerid Chott
Douz
Dahar
Algeria
Redjime Mâatoug
Nefzaoua Basin
Great Oriental Erg
0
40 Km
U- concentration (ppb)
19
18
17
16
15
14
13
12
11
10
9
8
7
6
5
4
3
2
1
Turonian Aquifer
Senonian Aquifer
Mio-Pliocene Aquifer of Redjime Mâatoug
Mio-Pliocene Aquifer of Tozeur basin
Mio-Pliocene Aquifer of Chott El Gharsa plain
Nefzaoua Basin
Djerid Basin
Phosphate ore of Tozeur-Nefta
Oasis
Localities
Uplands
Chotts

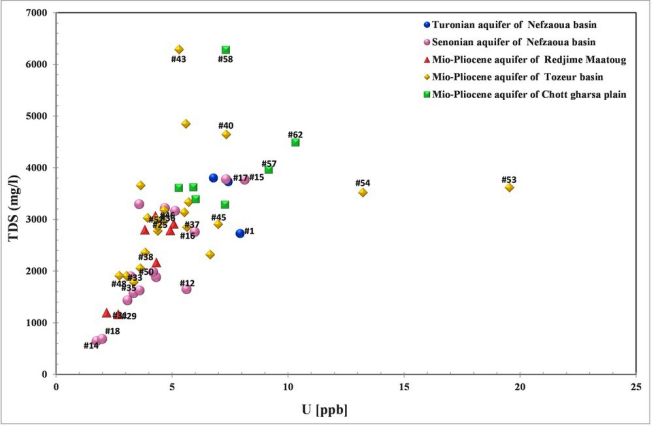
Turonian aquifer of Nefzaoua basin
Senonian aquifer of Nefzaoua basin
Mio-Pliocene aquifer of Redjime Maatoug
Mio-Pliocene aquifer of Tozeur basin
Mio-Pliocene aquifer of Chott gharsa plain
TDS (mg/l)
U [ppb]

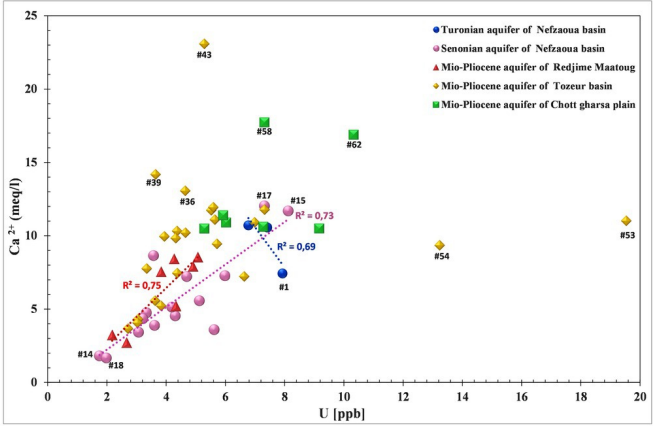
Turonian aquifer of Nefzaoua basin
Senonian aquifer of Nefzaoua basin
Mio-Pliocene aquifer of Redjime Maatoug
Mio-Pliocene aquifer of Tozeur basin
Mio-Pliocene aquifer of Chott gharsa plain
Ca 2+ (meq/l)
U [ppb]
R² = 0,73
R² = 0,69
R² = 0,75

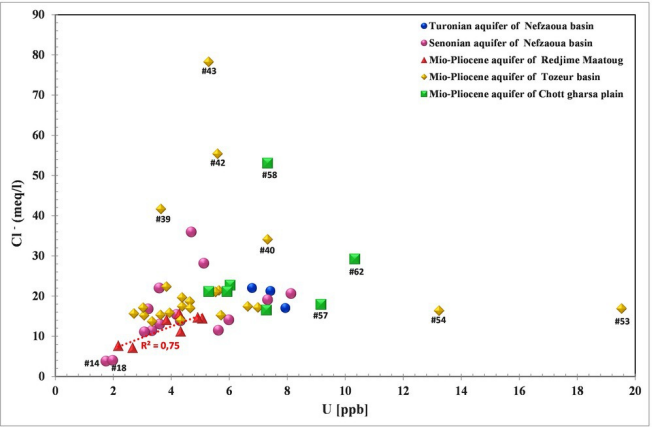
Turonian aquifer of Nefzaoua basin
Senonian aquifer of Nefzaoua basin
Mio-Pliocene aquifer of Redjime Maatoug
Mio-Pliocene aquifer of Tozeur basin
Mio-Pliocene aquifer of Chott gharsa plain
Cl - (meq/l)
U [ppb]
R² = 0,75

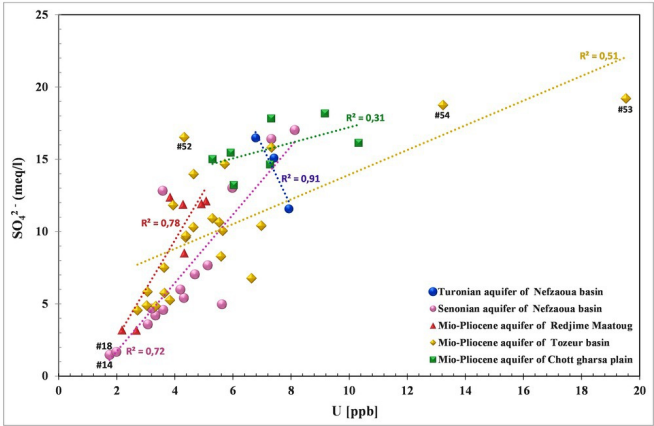
Turonian aquifer of Nefzaoua basin
Senonian aquifer of Nefzaoua basin
Mio-Pliocene aquifer of Redjime Maatoug
Mio-Pliocene aquifer of Tozeur basin
Mio-Pliocene aquifer of Chott gharsa plain
SO4 2- (meq/l)
U [ppb]
R² = 0,51
R² = 0,31
R² = 0,91
R² = 0,78
R² = 0,72

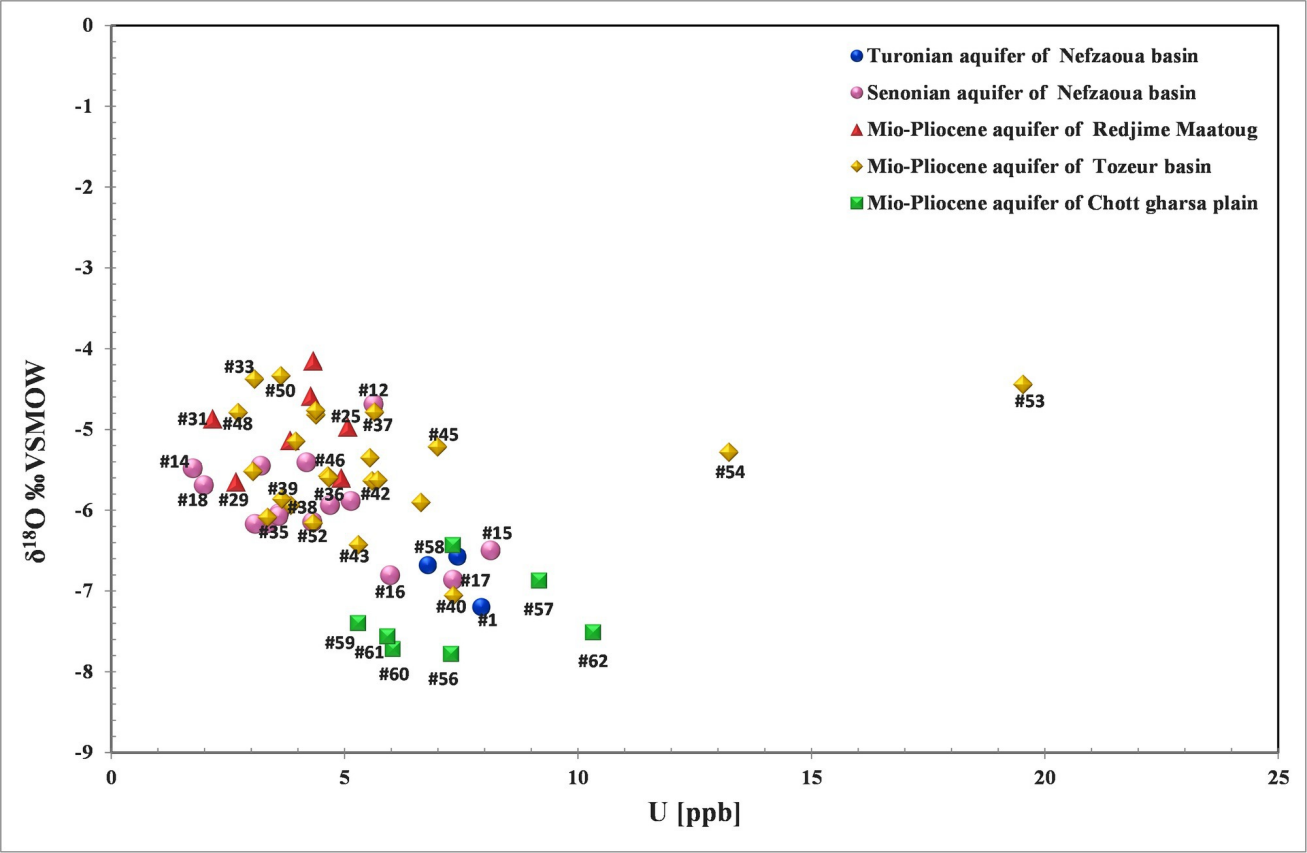
Turonian aquifer of Nefzaoua basin
Senonian aquifer of Nefzaoua basin
Mio-Pliocene aquifer of Redjime Maatoug
Mio-Pliocene aquifer of Tozeur basin
Mio-Pliocene aquifer of Chott gharsa plain
δ18O ‰VSMOW
U [ppb]
0
-1
-2
-3
-4
-5
-6
-7
-8
-9
0
5
10
15
20
25
#1
#12
#14
#15
#16
#17
#18
#25
#29
#31
#33
#35
#36
#37
#38
#39
#40
#42
#43
#45
#46
#48
#50
#52
#53
#54
#56
#57
#58
#59
#60
#61
#62

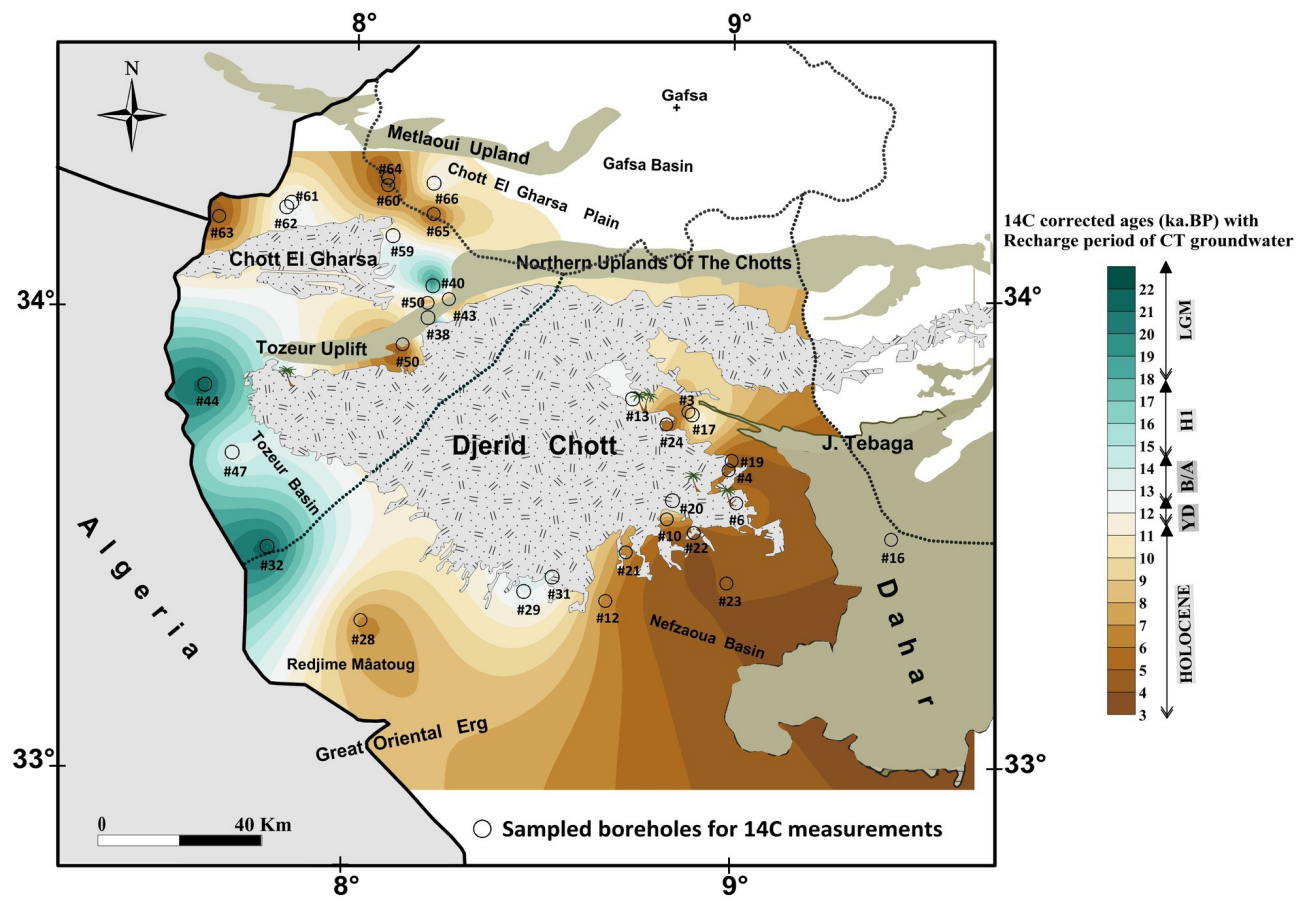
8°
9°
34°
33°
N
Gafsa
Metlaoui Upland
Gafsa Basin
Chott El Gharsa Plain
Chott El Gharsa
Northern Uplands Of The Chotts
Tozeur Uplift
Djerid Chott
J. Tebaga
Tozeur Basin
Algeria
Dahar
Nefzaoua Basin
Redjime Mâatoug
Great Oriental Erg
#60
#61
#62
#63
#64
#65
#66
#59
#40
#50
#43
#38
#44
#47
#32
#28
#29
#31
#12
#21
#22
#10
#20
#6
#4
#19
#24
#17
#3
#13
#16
#23
0
40 Km
Sampled boreholes for 14C measurements
14C corrected ages (ka.BP) with
Recharge period of CT groundwater
22
21
20
19
18
17
16
15
14
13
12
11
10
9
8
7
6
5
4
3
LGM
H1
B/A
YD
HOLOCENE

Table1. Field parameters and chemical results of analyzed groundwater samples of the CT aquifer in Chott Region (**Ɵ**).

Sample Labels	Aquifer	Basin	T ° C	pH	Screen depth (m)	Cl^- (meq/l)	NO_3^- (meq/l)	SO_4^{2-} (meq/l)	HCO_3^- (meq/l)	Na^+ (meq/l)	K^+ (meq/l)	Mg^{2+} (meq/l)	Ca^{2+} (meq/l)	TDS (mg/l)	Ionic Balance	SI Calcite	SI Dolomite
#1	Turonian	Nefzaoua	26,7	7,4	422	17,0	0,6	11,6	2,0	15,9	0,5	5,3	7,4	2726	-2%	0,18	0,34
#2	Turonian	Nefzaoua	26,1	7,6	33	21,3	0,3	15,1	2,3	19,3	0,5	6,3	10,6	3729	0%	0,53	0,96
#3	Turonian	Nefzaoua	26,1	7,25	44	22,0	0,8	16,5	2,2	19,3	0,5	6,3	10,7	3801	-4%	0,16	0,21
#4	Senonian	Nefzaoua	22,9	8,05	87	11,4	0,4	4,2	1,9	9,1	0,3	3,0	4,7	1573	4%	0,68	1,25
#5	Senonian	Nefzaoua	25,0	8,11	48	35,9	0,6	7,0	1,9	26,6	0,6	5,8	7,2	3219	1%	0,82	1,68
#6	Senonian	Nefzaoua	24,1	8,01	60	16,8	0,5	4,7	1,8	12,6	0,4	3,2	4,3	1898	-1%	0,57	1,12
#7	Senonian	Nefzaoua	25,1	8,21	89	13,0	0,4	4,6	2,1	9,9	0,3	2,9	3,9	1624	-2%	0,81	1,61
#8	Senonian	Nefzaoua	25,7	8	102	13,9	0,7	5,4	2,2	10,7	0,4	3,3	4,5	1882	-1%	0,68	1,36
#9	Senonian	Nefzaoua	24,6	8,16	59	11,1	0,5	3,6	2,1	9,0	0,3	2,6	3,4	1434	1%	0,73	1,45
#10	Senonian	Nefzaoua	26,5	7,85	103	15,4	0,5	6,0	2,2	12,6	0,4	3,5	5,1	1983	0%	0,59	1,14
#11	Senonian	Nefzaoua	24,0	8,1	37	28,2	0,9	7,7	2,2	23,7	0,6	5,2	5,6	3164	-1%	0,77	1,61
#12	Senonian	Nefzaoua	24,8	8,09	88	11,5	0,5	5,0	1,8	9,7	0,3	2,7	3,6	1649	-4%	0,59	1,17
#13	Senonian	Nefzaoua	25,5	7,9	92	22,0	0,3	12,8	2,6	19,3	0,7	5,1	8,6	3294	-3%	0,81	1,5
#14	Senonian	Nefzaoua	22,0	7,9	49	3,8	1,0	1,5	1,8	3,4	0,2	1,0	1,8	648	-1%	0,22	0,29
#15	Senonian	Nefzaoua	25,1	7,75	80	20,6	0,4	17,0	1,9	20,7	0,4	6,3	11,7	3769	0%	0,6	1,06
#16	Senonian	Nefzaoua	20,4	8,28	165	14,1	0,8	13,0	2,2	15,5	0,5	6,0	7,3	2757	-1%	0,88	1,66
#17	Senonian	Nefzaoua	25,7	7,78	58	19,1	0,2	16,4	2,0	21,4	0,5	6,4	12,0	3776	3%	0,68	1,21
#18	Senonian	Nefzaoua	25,0	7,7	52	4,0	0,5	1,7	1,8	4,5	0,0	1,1	1,7	687	-3%	0,02	-0,02
#19	Senonian	Nefzaoua	24,7	7,98	271	13,3	0,5	10,5	2,0	9,2	0,3	5,6	8,8	1599	-4%	0,6	1,12
#20	Senonian	Nefzaoua	25,6	8,08	91	12,0	0,2	10,2	2,0	9,7	0,3	6,4	8,6	1723	0%	0,7	1,4
#21	Senonian	Nefzaoua	24,7	8,04	109	14,4	0,7	8,1	2,0	10,6	0,4	7,6	8,9	1719	4%	0,67	1,4
#22	Senonian	Nefzaoua	26,0	8	80	15,0	0,3	27,5	2,4	15,0	0,3	11,3	18,2	3046	-1%	-0,47	-0,96
#23	Senonian	Nefzaoua	22,3	8,09	60	77,1	0,0	24,1	2,0	52,4	1,1	12,9	36,6	7000	0%	1,06	1,77

#24	Senonian	Nefzaoua	26,5	8,06	47	12,6	0,5	14,7	2,0	11,6	0,3	7,7	9,7	2017	-2%	0,7	1,44
#25	Mio-Pliocene	Redjime Mâatoug	26,8	7,76	225	14,5	0,5	12,1	2,4	14,0	0,6	6,1	8,5	2917	3%	0,66	1,31
#26	Mio-Pliocene	Redjime Mâatoug	26,7	7,96	180	14,7	0,6	11,9	2,3	14,1	0,6	6,0	7,9	2791	2%	0,65	1,3
#27	Mio-Pliocene	Redjime Mâatoug	25,5	7,99	165	14,1	0,2	12,4	1,1	13,2	0,6	4,7	7,6	2805	-3%	0,47	0,85
#28	Mio-Pliocene	Redjime Mâatoug	26,0	7,88	164	11,3	0,5	8,5	2,2	10,9	0,5	4,5	5,2	2171	-1%	0,58	1,22
#29	Mio-Pliocene	Redjime Mâatoug	22,4	8,25	118	7,2	0,2	3,2	2,0	6,8	0,4	2,1	2,7	1167	1%	0,7	1,38
#30	Mio-Pliocene	Redjime Mâatoug	22,7	7,76	190	15,6	0,5	11,9	3,6	14,9	0,8	5,1	8,4	3070	-1%	0,78	1,43
#31	Mio-Pliocene	Redjime Mâatoug	22,8	8,48	150	7,7	0,2	3,2	2,8	7,5	0,6	1,3	3,2	1199	0%	0,86	1,7
#32	Mio-Pliocene	Tozeur	25,8	7,53	287	15,8	0,1	11,8	2,7	14,0	0,7	5,2	10,0	3028	3%	0,54	0,92
#33	Mio-Pliocene	Tozeur	29,9	7,68	279	15,2	0,2	5,8	2,1	12,8	0,4	3,0	4,3	1896	-2%	0,37	0,75
#34	Mio-Pliocene	Tozeur	28,4	7,43	85	22,3	0,2	5,3	1,9	16,4	1,4	3,5	5,2	2361	0%	0,15	0,29
#35	Mio-Pliocene	Tozeur	34,8	7,6	500	13,7	0,2	4,8	1,9	8,6	0,2	1,3	7,8	1786	3%	0,59	0,6
#36	Mio-Pliocene	Tozeur	31,7	7,33	492	18,7	0,2	10,3	2,4	9,3	0,4	4,9	13,1	2961	4%	0,51	0,76
#37	Mio-Pliocene	Tozeur	29,8	7,45	362	21,4	0,3	10,1	2,3	15,6	0,3	4,9	11,1	2853	1%	0,51	0,83
#38	Mio-Pliocene	Tozeur	31,7	7,6	98	17,1	0,2	4,9	1,8	12,9	0,4	3,0	4,1	1909	4%	0,24	0,54
#39	Mio-Pliocene	Tozeur	32,4	7,34	550	41,7	0,2	5,7	2,0	21,8	0,4	4,1	14,2	3658	3%	0,49	0,64
#40	Mio-Pliocene	Tozeur	30,4	7,16	40	34,1	0,2	15,8	2,2	26,4	0,0	7,4	11,8	4646	-2%	0,15	0,26
#41	Mio-Pliocene	Tozeur	36,2	7,29	666	21,0	0,3	10,6	2,2	16,3	0,3	4,2	11,7	3139	4%	0,43	0,61
#42	Mio-Pliocene	Tozeur	31,9	7,18	64	55,4	0,5	8,3	2,1	35,8	0,8	6,2	11,9	4851	-1%	0,23	0,36
#43	Mio-Pliocene	Tozeur	33,1	7,17	64	78,3	0,2	10,9	2,3	49,2	1,0	8,0	23,1	6290	4%	0,48	0,7
#44	Mio-Pliocene	Tozeur	28,5	7,3	312	17,5	0,3	9,6	2,4	15,4	0,1	2,5	10,3	2777	3%	0,34	0,22
#45	Mio-Pliocene	Tozeur	32,8	7,17	275	17,2	0,2	10,4	2,2	13,3	0,2	4,0	10,9	2907	4%	0,24	0,24
#46	Mio-Pliocene	Tozeur	31,1	7,14	70	17,0	0,0	14,0	2,3	14,2	0,0	5,5	10,2	3184	-2%	0,15	0,19
#47	Mio-Pliocene	Tozeur	26,8	7,42	443	19,6	0,3	9,7	2,4	16,3	0,0	4,8	7,4	2859	-1%	0,29	0,52
#48	Mio-Pliocene	Tozeur	29,3	7,33	285	15,6	0,1	4,6	2,0	16,3	0,0	2,6	3,7	1911	4%	0,64	1,21
#49	Mio-Pliocene	Tozeur	31,5	7,55	300	17,4	0,2	6,8	2,2	13,4	0,4	3,9	7,2	2321	4%	0,48	0,86
#50	Mio-Pliocene	Tozeur	30,0	8,1	320	15,3	0,3	7,5	2,3	15,5	0,5	3,4	5,6	2058	2%	0,89	1,73
#51	Mio-Pliocene	Tozeur	29,0	7,2	68	15,2	0,1	14,7	2,0	15,8	0,6	6,1	9,4	3336	1%	0,03	-0,02

#52	Mio-Pliocene	Tozeur	30,0	7,22	612	14,0	0,0	16,5	2,0	12,6	0,7	6,2	9,8	3002	-4%	0,12	0,18
#53	Mio-Pliocene	Tozeur	28,2	8,02	65	16,9	0,2	19,2	3,4	17,2	0,8	6,4	11,0	3617	-4%	1,07	2,01
#54	Mio-Pliocene	Tozeur	27,0	7,8	100	16,4	0,2	18,8	2,4	17,9	0,7	7,1	9,4	3522	-4%	-0,14	-0,29
#55	Mio-Pliocene	Tozeur	30,0	7,28	482	13,3	0,3	17,0	2,2	12,9	0,5	8,2	12,0	2138	1%	0,09	0,19
#56	Mio-Pliocene	Chott El Gharsa Plain	30,0	7,9	565	16,5	0,1	14,6	2,4	20,2	0,0	4,9	10,6	3284	3%	0,89	1,61
#57	Mio-Pliocene	Chott El Gharsa Plain	30,0	7,2	500	17,9	0,0	18,2	2,4	26,3	0,4	4,9	10,5	3961	1%	0,17	0,17
#58	Mio-Pliocene	Chott El Gharsa Plain	35,9	7,8	538	53,1	0,0	17,8	2,4	40,5	1,0	10,3	17,7	6279	4%	1	1,98
#59	Mio-Pliocene	Chott El Gharsa Plain	49,0	8	1052	21,1	0,1	15,0	2,4	25,6	0,0	4,6	10,5	3610	2%	1,13	2,12
#60	Mio-Pliocene	Chott El Gharsa Plain	39,8	8,1	1174	22,7	0,1	13,2	2,4	22,1	0,0	5,1	10,9	3392	2%	1,2	2,28
#61	Mio-Pliocene	Chott El Gharsa Plain	45,0	7,6	1052	21,1	0,1	15,5	2,3	15,8	0,4	5,7	11,4	3622	-4%	0,79	1,49
#62	Mio-Pliocene	Chott El Gharsa Plain	42,0	7,2	1164	29,2	0,1	16,1	2,5	17,9	0,5	8,1	16,9	4489	3%	0,55	0,99
#63	Mio-Pliocene	Chott El Gharsa Plain	45,8	8,19	1081	28,0	0,0	29,0	4,1	28,2	0,5	19,7	14,4	3700	1%	1,36	3,11
#64	Mio-Pliocene	Chott El Gharsa Plain	41,0	7,8	846	34,4	0,0	32,2	2,0	32,2	0,0	10,8	25,4	4500	-1%	0,88	1,61
#65	Mio-Pliocene	Chott El Gharsa Plain	30,0	7,9	660	24,0	0,0	39,4	2,8	20,0	0,5	12,6	31,0	4650	-2%	1,05	1,88
#66	Mio-Pliocene	Chott El Gharsa Plain	35,0	7,8	565	50,1	0,0	43,4	1,9	52,0	0,7	22,9	25,6	7050	3%	0,73	1,6

Θ: Hadj Ammar et al., 2014.

Table 2. Uranium isotopic data together with stable isotopes and ^{14}C corrected age of analyzed groundwater samples of the CT aquifer.

Sample Labels	Aquifer	Basin	$\delta^{18}O$ ‰ vs SMOW ɵ	$\delta^{2}H$ ‰ vs SMOW ɵ	U (ppb) γ	U error	$^{234}U/^{238}U$ γ	$^{234}U/^{238}U$ error	^{14}C activity (pmC)	^{14}C error	$\delta^{13}C$ ‰ PDB	Corrected ^{14}C Age (Year)	Age standard deviation	A_0 Fontes and Garnier	Uncorrected 14C Age (Year)
#1	Turonian	Nefzaoua	-7,2	-54,5	7,927	0,014	1,386	0,002	30,2*	1,2	-7,3	1382	247,2	35,7	9898
#2	Turonian	Nefzaoua	-6,6	-50,5	7,413	0,014	1,767	0,003	na	na	na	na	na	na	na
#3	Turonian	Nefzaoua	-6,7	-50,4	6,778	0,013	1,652	0,003	11,2*	1,0	-4,5	5112	671,7	20,8	18099
#4	Senonian	Nefzaoua	-6,2	-51,7	3,334	0,007	1,732	0,006	18,1γ	1,3	-5,1	2531	435,4	24,6	14130
#5	Senonian	Nefzaoua	-5,9	-44,8	4,691	0,008	1,537	0,003	na	na	na	na	na	na	na
#6	Senonian	Nefzaoua	-5,4	-45,8	3,204	0,005	1,669	0,002	10,8ε	0,9	-3,6	3508	477,4	16,5	18399
#7	Senonian	Nefzaoua	-6,0	-49,9	3,600	0,006	1,740	0,002	na	na	na	na	na	na	na
#8	Senonian	Nefzaoua	-6,1	-50,9	4,304	0,007	1,808	0,003	na	na	na	na	na	na	na
#9	Senonian	Nefzaoua	-6,2	-48,7	3,071	0,005	1,695	0,002	na	na	na	na	na	na	na
#10	Senonian	Nefzaoua	-5,4	-51,5	4,186	0,008	1,879	0,002	11,6ε	1,2	-5,8	7191	714,4	27,7	17808
#11	Senonian	Nefzaoua	-5,9	-46,2	5,126	0,010	1,691	0,003	na	na	na	na	na	na	na
#12	Senonian	Nefzaoua	-4,7	-46,8	5,623	0,010	1,605	0,003	9,6ε	1,1	-4,6	6719	864,2	21,6	19373
#13	Senonian	Nefzaoua	-6,1	-48,8	3,577	0,006	1,776	0,003	6,7γ	1,0	-5,2	10842	1243,1	24,9	22346
#14	Senonian	Nefzaoua	-5,5	-41,6	1,749	0,003	1,492	0,002	na	na	na	na	na	na	na
#15	Senonian	Nefzaoua	-6,5	-49,0	8,121	0,016	1,833	0,003	na	na	na	na	na	na	na

#16	Senonian	Nefzaoua	-6,8	-51,1	5,978	0,014	1,518	0,003	17,9[γ]	2,0	-4,2	1055	462,3	20,3	14222
#17	Senonian	Nefzaoua	-6,9	-51,0	7,316	0,014	1,732	0,002	6,9[γ]	1,2	-6,2	12157	1206,5	30,0	22103
#18	Senonian	Nefzaoua	-5,7	-45,2	1,981	0,003	1,134	0,002	na	na	na	na	na	na	na
#19	Senonian	Nefzaoua	-6,2	-53,9	na	na	na	na	17,7[γ]	1,1	-4,8	2043	467,5	22,7	14315
#20	Senonian	Nefzaoua	-6,2	-50,7	na	na	na	na	8,8[γ]	1,0	-7,9	12261	943,4	38,8	20092
#21	Senonian	Nefzaoua	-6,1	-48,6	na	na	na	na	12,4[γ]	1,1	-4,6	5135	668,1	23,1	17257
#22	Senonian	Nefzaoua	-6,3	-50,9	na	na	na	na	na	na	na	na	na	na	na
#23	Senonian	Nefzaoua	-6,0	-49,5	na	na	na	na	20,7[γ]	1,3	-6,5	3497	505,9	31,6	13021
#24	Senonian	Nefzaoua	-5,7	-51,3	na	na	na	na	16,4[γ]	1,4	-6,8	5787	613,4	33,0	14946
#25	Mio-Pliocene	Redjime Mâatoug	-5,0	-47,8	5,071	0,009	3,140	0,004	na	na	na	na	na	na	na
#26	Mio-Pliocene	Redjime Mâatoug	-5,6	-49,1	4,913	0,009	2,831	0,003	na	na	na	na	na	na	na
#27	Mio-Pliocene	Redjime Mâatoug	-5,1	-49,4	3,828	0,006	2,704	0,003	na	na	na	na	na	na	na
#28	Mio-Pliocene	Redjime Mâatoug	-4,1	-44,4	4,324	0,007	2,705	0,003	10,3[γ]	1,5	-7,7	10713	940,6	37,6	18791
#29	Mio-Pliocene	Redjime Mâatoug	-5,6	-53,5	2,667	0,004	2,134	0,002	6,9[ε]	1,0	-5,9	11766	1890,6	28,6	22103
#30	Mio-Pliocene	Redjime Mâatoug	-4,6	-46,7	4,279	0,007	2,805	0,003	na	na	na	na	na	na	na
#31	Mio-Pliocene	Redjime Mâatoug	-4,9	-45,5	2,176	0,004	1,833	0,003	7,1[γ]	0,9	-7,4	13509	1172,1	36,4	21867
#32	Mio-Pliocene	Tozeur	-5,1	-40,1	3,942	0,008	2,685	0,005	1,75[γ]	1	-6,8	24252	5655,5	32,9	33445
#33	Mio-Pliocene	Tozeur	-4,4	-45,1	3,059	0,006	2,237	0,006	na	na	na	na	na	na	na
#34	Mio-Pliocene	Tozeur	-5,9	-50,9	3,833	0,008	2,365	0,004	na	na	na	na	na	na	na

#35	Mio-Pliocene	Tozeur	-6,1	-34,8	3,337	0,007	2,361	0,007	na	na	na	na	na	na	na
#36	Mio-Pliocene	Tozeur	-5,6	-39,8	4,638	0,012	3,177	0,009	na	na	na	na	na	na	na
#37	Mio-Pliocene	Tozeur	-4,8	-45,8	5,641	0,013	2,584	0,006	na	na	na	na	na	na	na
#38	Mio-Pliocene	Tozeur	-5,5	-40,2	3,034	0,007	2,162	0,005	2,1[γ]	1	-7,0	22921	5407,7	33,6	31937
#39	Mio-Pliocene	Tozeur	-5,9	-51,7	3,644	0,007	2,787	0,004	na	na	na	na	na	na	na
#40	Mio-Pliocene	Tozeur	-7,1	-53,1	7,323	0,017	1,798	0,004	3,68[γ]	1,2	-10,8	22142	3329,9	53,6	27300
#41	Mio-Pliocene	Tozeur	-5,3	-46,2	5,529	0,014	2,218	0,007	na	na	na	na	na	na	na
#42	Mio-Pliocene	Tozeur	-5,6	-50,7	5,592	0,013	2,314	0,007	na	na	na	na	na	na	na
#43	Mio-Pliocene	Tozeur	-6,4	-48,5	5,289	0,050	2,452	0,067	11,5[γ]	0,9	-5,7	6968	922,3	26,7	17880
#44	Mio-Pliocene	Tozeur	-4,8	-45,4	4,374	0,011	2,610	0,008	3,2[γ]	0,8	-6,4	18636	3066,6	30,5	28455
#45	Mio-Pliocene	Tozeur	-5,2	-48,1	6,979	0,017	2,055	0,006	na	na	na	na	na	na	na
#46	Mio-Pliocene	Tozeur	-5,6	-44,3	4,652	0,011	2,852	0,007	na	na	na	na	na	na	na
#47	Mio-Pliocene	Tozeur	-4,8	-46,4	4,379	0,009	2,782	0,005	5,8[γ]	1,2	-7,5	15192	2193,2	36,4	23539
#48	Mio-Pliocene	Tozeur	-4,8	-44,9	2,713	0,006	2,169	0,006	na	na	na	na	na	na	na
#49	Mio-Pliocene	Tozeur	-5,9	-46,8	6,639	0,019	2,246	0,009	na	na	na	na	na	na	na
#50	Mio-Pliocene	Tozeur	-4,3	-42,0	3,627	0,009	2,645	0,008	18,3[γ]	1,0	-8,3	6645	524,4	40,9	14040
#51	Mio-Pliocene	Tozeur	-5,6	-49,6	5,714	0,013	2,833	0,006	17,8[γ]	1,6	-6,1	4103	933,3	29,2	14269
#52	Mio-Pliocene	Tozeur	-6,2	-52,5	4,319	0,010	3,121	0,007	na	na	na	na	na	na	na
#53	Mio-Pliocene	Tozeur	-4,4	-45,5	19,530	0,051	2,491	0,007	na	na	na	na	na	na	na

#54	Mio-Pliocene	Tozeur	-5,3	-45,9	13,228	0,020	2,452	0,007	na	na	na	na	na	na	na
#55	Mio-Pliocene	Tozeur	-4,2	-42,8	na	na	na	na	na	na	na	na	na	na	na
#56	Mio-Pliocene	Chott El Gharsa Plain	-7,8	-54,9	7,281	0,014	1,641	0,004	24,9[i]	2,0	-7,9	3338	831,1	38,8	11168
#57	Mio-Pliocene	Chott El Gharsa Plain	-6,9	-51,5	9,165	0,017	1,340	0,003	na	na	na	na	na	na	na
#58	Mio-Pliocene	Chott El Gharsa Plain	-6,4	-49,5	7,316	0,014	2,786	0,006	na	na	na	na	na	na	na
#59	Mio-Pliocene	Chott El Gharsa Plain	-7,4	-56,4	5,296	0,011	1,572	0,005	7,3[i]	0,8	-6,4	12365	1129,6	36,6	20676
#60	Mio-Pliocene	Chott El Gharsa Plain	-7,7	-52,9	6,024	0,011	1,654	0,004	8,4[i]	0,5	-8,2	6453	694,3	40,2	13995
#61	Mio-Pliocene	Chott El Gharsa Plain	-7,6	-57,4	5,920	0,011	1,611	0,005	6,3[i]	0,5	-8,7	15806	1170,2	42,6	22855
#62	Mio-Pliocene	Chott El Gharsa Plain	-7,5	-54,9	10,328	0,022	1,408	0,006	7,5[i]	1,0	-8,8	14374	1439,6	42,7	21414
#63	Mio-Pliocene	Chott El Gharsa Plain	-5,8	-55,7	na	na	na	na	17,1[i]	1,4	-7,6	6320	776,4	36,7	14600
#64	Mio-Pliocene	Chott El Gharsa Plain	-7,3	-51,2	na	na	na	na	9,2[i]	1,6	-8,6	8477	590,4	42,2	15601
#65	Mio-Pliocene	Chott El Gharsa Plain	-7,7	-51,0	na	na	na	na	18[i]	1,0	-7,5	5882	710,3	36,7	14176
#66	Mio-Pliocene	Chott El Gharsa Plain	-7,1	-49,0	na	na	na	na	6,5[i]	1,2	-6,4	12797	1675,9	30,6	22597